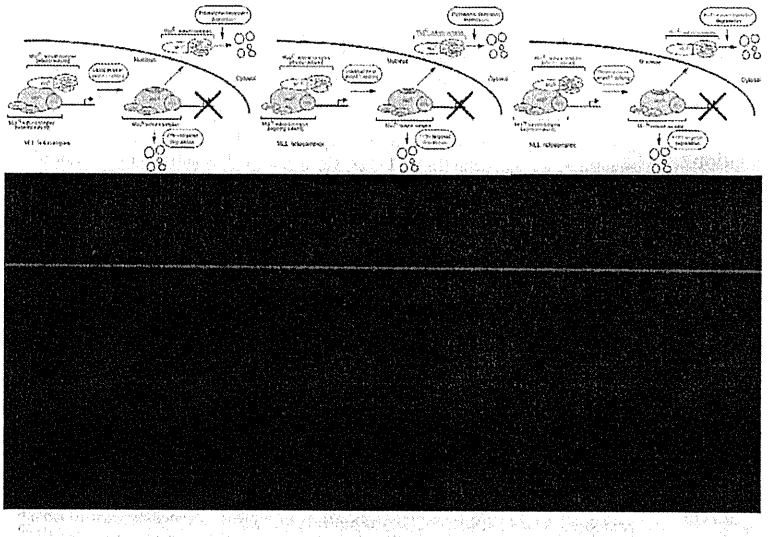

Fig. 7. A model of the two distinct degradation pathways for each MLL subunit.

progenitors and exhaustion of HSCs. Our analysis of the MLL-deficient hematopoietic system underscores a previously unappreciated role for MLL in LSK $CD48^{+}Flk2^{+}$ cells, which is consistent with *Hoxa9* being most highly expressed in MPPs (Forsberg et al., 2005) and could account for the inability of *dC/dC* fetal liver cells to reconstitute the hematopoietic system, even short-term, despite seemingly intact differentiation capacities. Hence, MLL^{C} is crucial to early stages of hematopoietic development.

From these results we conclude that the MLL holocomplex is responsible for MLL-dependent transcription because MLL^{C} is required in three different biological processes including embryogenesis, maintenance of cellular homeostasis in fibroblasts and hematopoietic development.

MLL subunits are subjected to distinct degradation mechanisms upon dissociation

We observed that free Mll^{N} was undetectable in *dC* homozygous MEFs despite comparable expression of *Mll* mRNAs. Furthermore, Mll^{C}-deficient embryos expressed only minimal amounts of Mll^{N}. These results indicate that free MLL^{N} is degraded by a post-transcriptional mechanism in vivo. In this study, we discovered that free MLL^{C} is exported to the cytosol and degraded via a proteasome-dependent pathway. Thus, both of the MLL subunits generated by processing are unstable if not forming an MLL holocomplex. Free MLL^{N} is destroyed by a unique mechanism that targets the FYRN domain. This degradation mechanism appears to be independent of the proteasome degradation pathway and therefore should be different from the previously reported SCF- or APC-proteasome-dependent mechanisms that dynamically regulate MLL protein levels during the cell cycle, which targets a different portion of MLL (amino acids 1–1400) (Liu et al., 2007). It is unclear at this point how free MLL^{N} fragments are degraded. It might involve autophagic degradation similar to the piecemeal microautophagy of the nucleus observed in yeast (Krick et al., 2009) or 'nucleophagy' observed in mammalian cells (Park et al., 2009).

FYRN domains are often found adjacent to FYRC in SET domain-containing proteins and together constitute a DAST domain, which is evolutionarily conserved between humans and plants (Alvarez-Venegas and Avramova, 2001). The FYRN domain directly associates with the FYRC domain through the hydrophobic residues of each domain, thereby its interaction surface is kept unexposed (Garcia-Alai et al., 2010; Pless et al., 2011; Hsieh et al., 2003b). Our data suggest that the FYRN domain harbors a destabilization signal that is normally masked by MLL^{C} within the MLL holocomplex. Supporting this notion, deletion of FYRN did not render MLL^{N} unstable, despite an inability to associate with MLL^{C}. The ability of FYRN to destabilize the MLL-AF9 protein and inactivate its transcriptional and oncogenic properties is consistent with this proposal and probably accounts for the absence of chromosomal translocations downstream of the FYRN domain in human leukemias (Meyer et al., 2009). Hence, FYRN might serve not only as a platform for interaction with FYRC but also as a destabilization signal that activates the targeted destruction process when exposed. The exposed hydrophobic surface of FYRN might trigger aggregation of the free MLL^{N} fragment, which is then subjected to autophagic degradation (Knaevelsrud and Simonsen, 2010).

Because free MLL^{N} is degraded if it is dissociated from MLL^{C}, it is unlikely to possess any biological functions. However, free MLL^{N} might have functions in circumstances where the degradation pathway is inhibited. In *Drosophila*, it has been suggested that TRX^{N} associates with the genome without TRX^{C} at some loci. Whether MLL^{N} and MLL^{C} also differently associate with the human genome is currently unknown. Our data show that there is an intrinsic regulatory mechanism that effectively extinguishes MLL^{N} upon loss of intramolecular interaction. Therefore MLL^{N} must be protected from the degradation mechanism in order to function without MLL^{C} if it has a biological function (Fig. 7).

PHD1 is necessary for holocomplex formation and implicated in tumor suppression

Our structure–function analysis revealed that PHD1 and PHD4 are crucial for intramolecular interaction in the context of the full-length protein. PHD fingers serve as protein–protein interaction motifs (Fair et al., 2001). Recently, it has been shown that PHD3 specifically associates with di- and tri-methylated lysine 4 of histone H3 (Milne et al., 2010; Wang et al., 2010b; Chang et al., 2010). It is possible that PHD1 and/or PHD4 bind to specific motifs within MLL to enable or stabilize physical interaction between FYRN and FYRC. Such interactions could be modulated

through post-translational modifications such as lysine methylation, thereby providing opportunities for a context-dependent regulation of holocomplex formation.

We demonstrate here that exclusion of exon 11 sequences from the *MLL* mRNA produces a variant protein lacking PHD1 that is unable to associate with MLL^C, and thus subjected to degradation. Because the Δexon11 transcript is present in both normal and leukemia cells (Löchner et al., 1996; Nam et al., 1996; Takeuchi et al., 2008), alternative splicing of exon 11 might provide another context-dependent mechanism to conditionally extinguish MLL activity in vivo.

Genomic deletion and enhanced alternative splicing of *MLL* exon 11 have been reported in a subset of acute lymphoid leukemias (Löchner et al., 1996). Because exon 11 deletion abolishes holocomplex formation and renders MLL nonfunctional, its oncogenic mechanism should differ from MLL-fusion-associated leukemias, in which a gain-of-function mechanism plays the predominant role (Ayton and Cleary, 2001; Hess, 2004; Krivtsov and Armstrong, 2007). This raises the possibility that MLL serves as a tumor suppressor in the lymphoid lineage. In endocrine tissues, inactivating mutations of menin prevent the MLL–menin complex maintaining appropriate expression of *Cdkn1b* and *Cdkn2c* as part of a negative growth regulatory and tumor suppressor transcriptional circuit (Franklin et al., 1998; Franklin et al., 2000; Karnik et al., 2005; Milne et al., 2005). Indeed, these CDKIs are expressed at very low levels in *dC/dC* MEFs. These CDKIs have also been implicated in lymphoid growth control and tumorigenesis. Lymphoid cells from *Cdkn2c* knockout mice are hyper-proliferative to mitogens (Franklin et al., 1998), and inactivating mutations of *Cdkn1b* have been reported in T-ALL and other types of leukemia (Le Toriellec et al., 2008; Markaki et al., 2006). The Notch1 pathway, which is activated frequently in T-ALL, effectively reduces CDKN1B levels through upregulation of SKP2 expression (Dohda et al., 2007). Collectively, these data suggest that deletion of exon 11 might contribute to oncogenesis by downregulating CDKIs in lymphoid cells. Thus MLL might function as a tumor suppressor in the lymphoid lineage with a mechanism similar to that in endocrine tissues. However, conditional knockout studies show that *Mll* deficiency does not cause immediate expansion of lymphoid lineage populations (Jude et al., 2007; McMahon et al., 2007). These results do not support a rate-limiting role of MLL for proliferation of lymphoid cells, and suggest that additional mutations might be required for full transformation. Further investigation is required to determine whether MLL truly serves a tumor suppressor role in lymphoid lineages.

In summary, our studies define a crucial role for holocomplex formation of MLL subunits in various developmental processes, which is necessary to protect MLL^N from the FYRN-targeted degradation mechanism. Our data suggest that if MLL^N were to function without MLL^C, the FYRN domain must be masked or modified to ensure MLL^N stability; however, our studies provide no evidence for separate MLL^N function in various MLL-dependent processes.

Materials and Methods

Cell culture

293T, plat-E and MEF cells were cultured in Dulbecco's modified Eagle's medium supplemented with 15% fetal calf serum and non-essential amino acids.

Subfractionation, immunoprecipitation and western blotting

Preparation of nuclear extracts, immunoprecipitation (IP) and western blotting were performed as described previously (Yokoyama et al., 2004). Primary antibodies included mouse monoclonal anti-MLL^N (mmN4.4), anti-MLL^C (mmC2.1), anti-Sbf-1 (HAF3P.1) and polyclonal rabbit anti-MLL^N (rpN1) as described elsewhere (Yokoyama et al., 2002). Anti-HCF-1_C (H12) antibody was provided by Winship Herr. The mouse monoclonal anti-MLL^C (9–12) antibody was generated using maltose-binding protein (MBP) fusion protein corresponding to residues 3084–3959 of human MLL. Goat anti-menin (C19), mouse anti-GAL4 (RK5C1) and omni-probe (D-8; recognizes the nearby sequence of the Xpress epitope) antibodies were purchased from Santa Cruz Biotechnology, Inc. Additional primary antibodies included mouse anti-actin (MAB 1501R; Chemicon) and rat anti-HA (3F10; Roche). Agarose affinity beads coupled to mouse anti-FLAG (M2) monoclonal antibody were purchased from Sigma.

Construction of the expression vectors

Xpress–FLAG–MLL–HA expression vectors [pLNCX (Xf)MLL(H) and its derivatives] are described elsewhere (Yokoyama et al., 2002). Various MLL mutants were generated by polymerase chain reaction (PCR)-mediated mutagenesis and restriction enzyme digestion and/or ligation. The GAL4 DNA binding domain, Xpress epitope, 3xNLS and CFP and YFP portion were transferred from pM (Clontech), pcDNA4 Hix/Max (Invitrogen), pEF/myc/nuc/GFP (Invitrogen) and pECFP-C1/pEYFP-C1 (BD Biosciences) vectors, respectively. Assembled cDNAs were cloned into the pLNCX vector (Clontech). The various MLL-AF9 mutants were generated by modification of the pMSCV MLL-AF9 vector (Somervaille and Cleary, 2006).

Generation of knockin mice

A mouse ES BAC DNA pool (Down-to-the-well™) was screened by PCR to isolate a BAC clone containing the *Mll* locus. Targeting vectors containing neo and DT cassettes (kindly provided by Takeshi Yagi) were constructed by PCR-mediated mutagenesis, restriction enzyme digestion and ligation. ES cells (CGR8.8) were transfected with the linearized targeting vectors and screened for positive clones by PCR. Homologous recombination was confirmed by using the LA-PCR kit (Takara Bio Inc.) specific for both ends of the targeting construct (primer sequences available upon request). Targeted clones were transiently transfected with a Cre recombinase expression vector (kindly provided by Takeshi Yagi) and subsequently screened for clones with appropriate excision of the neo cassette. Diagnostic PCR for genotyping was performed using a primer pair of the forward primer: 5′-CTGGCATCATGTATTTTGAACAGGCACCCC-3′ and the reverse primer: 5′-TACACGTGGTAACCAGTCATCTGCAGCTCA-3′ by LA-PCR followed by digestion with *XhoI*. Blastocyst injections were performed by the Transgenic Research Facility of Stanford University. Germline transmission of the targeted *Mll* allele was confirmed by PCR genotype analysis. Knockin mouse lines were maintained by backcrossing onto a C57BL6 genetic background. p53 knockout mice were reported previously (Donehower et al., 1992).

Whole-mount in situ hybridization

In situ hybridization was performed on E10.5 embryos as described elsewhere (Capellini et al., 2006). Plasmids for probes were kindly provided by Licia Selleri.

Quantitative RT-PCR

Reverse transcription (RT) and quantitative PCR (qPCR) were performed as described previously (Yokoyama et al., 2005). Taqman probes for *Actb* (Mm00607939_s1), *Gapdh* (Mm99999915_g1), *Hoxa9* (Mm00439364_m1), *Hoxc4* (Mm00442838_m1), *Hoxc8* (Mm00439369_m1), *Hoxc9* (Mm00433972_m1), *Cdkn1b* (Mm00439167_g1), *Cdkn2c* (Mm00483243_m1), *Pml* (Mm00476969_m1), *Serpine1* (Mm00435860_m1), *Mll*(N) (Mm01179246_g1) and *Mll*(C) (Mm01179235_m1) were purchased from Applied Biosystems. qPCR was performed in triplicate and average expression levels (with standard deviations) normalized to that of *Gapdh* or β-actin gene were calculated using a standard curve and the relative quantification method as described in ABI User Bulletin #2.

MEF proliferation and 3T3 senescence assays

MEFs were derived from E11.5 embryos and handled as described elsewhere (Sage et al., 2000). In proliferation assay, 5×10^4 cells were plated in a 60 mm dish on day 0 and the cells were counted after trypsinization and resuspension in medium at each time point. In 3T3 senescence assays, 5×10^4 cells were replated in a 60 mm dish every 3 days.

Flow cytometry

Flow cytometry analysis was performed at the fluorescence-activated cell sorter (FACS) facility of Stanford University as previously described (Ficara et al., 2008). Fetal liver single-cell suspensions were stained in deficient Roswell Park Memorial Institute medium (RPMI; Irvine Scientific) containing 3% fetal calf serum, 1 mM EDTA and 0.01 M HEPES. Conjugated monoclonal antibodies were obtained from either BD Pharmingen (BD) or eBioscience (San Diego, CA). The lineage cocktail included Gr1 (RB6-8C5), B220 (RA3-6B2), TER119 (TER-119), CD3 (145-2C12), CD4 (GK1.5) and CD8. The following monoclonal antibodies were also used: Mac1/CD11b (M1/70), cKit (2B8), Sca1 (D7), CD48 (HM48-1), CD34 (49E8), CD16/32 (93), Flk2 (A2F10), CD45.2 (104) and CD43 (S7). Stained cells were analyzed with an LSR-1A or LSR-II flow cytometer. Cell Quest Pro or Diva (BD) were used for data acquisition, and FlowJo (Tree Star) was used for analysis.

Cytospin and in vitro differentiation to macrophages

Fetal liver cells were cultured for 1 week in methylcellulose medium (M3231; Stemcell Technologies; Vancouver, BC) containing SCF, IL-3, IL-6 and GM-CSF. Cytospin preparations were stained with May–Grunwald–Giemsa stain for assessment of cellular cytology as described elsewhere (Yokoyama et al., 2005).

In vivo reconstitution assay

Fetal liver cells from homozygous mutant (5×10^5 cells) or wt embryos (5×10^4 cells) were injected intravenously into lethally irradiated (900 rad) C57BL6 mice. Recipient mice were maintained on water supplemented with neomycin.

Myeloid progenitor transformation assay

The myeloid progenitor transformation assay was described elsewhere (Lavau et al., 1997; Yokoyama and Cleary, 2008). A portion of the cells was lysed at the end of the first round of plating to prepare RNA using an RNAeasy mini kit (Qiagen).

Indirect immunofluorescence

Indirect immunofluorescence was performed using 293T cells transfected with various *MLL* expression vectors as described elsewhere (Yokoyama and Cleary, 2008). Transfected cells were fixed and incubated with rabbit anti-MLL^N (rpN1) or mouse anti-Xpress (omni probe D-8) antibodies, and then probed with FITC-conjugated goat anti-rabbit IgG or TRED-conjugated anti-mouse IgG (Santa Cruz Biotechnology). Cells were stained with DAPI (Vector Laboratories) and analyzed by immunofluorescence microscopy.

We thank E. Allen and H. Zeng (Stanford Transgenic Research Facility) for technical support, T. Yagi and L. Selleri for plasmids, and W. Herr for an antibody. We acknowledge C. Nicolas, M. Ambrus, B. T. Rouse, C. Hatanaka and M. Kawaguchi for technical assistance, and A. James for graphics support. We thank L. Selleri, T. Capellini and J. Sage for technical instruction and helpful discussions. F.F. was supported by an ASH scholar award from the American Society of Hematology. These studies were supported by the Children's Health Initiative of the Packard Foundation and grants from the National Institutes of Health (CA55029 and CA116606) to M.L.C. and by a Grant-in-aid for Scientific Research on Innovative Areas (22118003) and a Grant-in-aid for the Third-Term Comprehensive 10-Year Strategy for Cancer Control to A.Y. Deposited in PMC for release after 12 months.

Supplementary material available online at
http://jcs.biologists.org/cgi/content/full/124/13/2208/DC1

References

Alvarez-Venegas, R. and Avramova, Z. (2001). Two Arabidopsis homologs of the animal trithorax genes: a new structural domain is a signature feature of the trithorax gene family. *Gene* **271**, 215-221.

Ayton, P. M. and Cleary, M. L. (2001). Molecular mechanisms of leukemogenesis mediated by MLL fusion proteins. *Oncogene* **20**, 5695-5707.

Ayton, P. M., Chen, E. H. and Cleary, M. L. (2004). Binding to nonmethylated CpG DNA is essential for target recognition, transactivation, and myeloid transformation by an MLL oncoprotein. *Mol. Cell. Biol.* **24**, 10470-10478.

Bertolino, P., Tong, W. M., Galendo, D., Wang, Z. Q. and Zhang, C. X. (2003). Heterozygous Men1 mutant mice develop a range of endocrine tumors mimicking multiple endocrine neoplasia type 1. *Mol. Endocrinol.* **17**, 1880-1892.

Birke, M., Schreiner, S., Garcia-Cuellar, M. P., Mahr, K., Titgemeyer, F. and Slany, R. K. (2002). The MT domain of the proto-oncoprotein MLL binds to CpG-containing DNA and discriminates against methylation. *Nucleic Acids Res.* **30**, 958-965.

Caldas, C., Kim, M. H., MacGregor, A., Cain, D., Aparicio, S. and Wiedemann, L. M. (1998). Isolation and characterization of a pufferfish MLL (mixed lineage leukemia)-like gene (fMll) reveals evolutionary conservation in vertebrate genes related to Drosophila trithorax. *Oncogene* **16**, 3233-3241.

Capellini, T. D., Di Giacomo, G., Salsi, V., Brendolan, A., Ferretti, E., Srivastava, D., Zappavigna, V. and Selleri, L. (2006). Pbx1/Pbx2 requirement for distal limb patterning is mediated by the hierarchical control of Hox gene spatial distribution and Shh expression. *Development* **133**, 2263-2273.

Caslini, C., Connelly, J. A., Serna, A., Broccoli, D. and Hess, J. L. (2009). MLL associates with telomeres and regulates telomeric repeat-containing RNA transcription. *Mol. Cell. Biol.* **29**, 4519-4526.

Chang, P. Y., Hom, R. A., Musselman, C. A., Zhu, L., Kuo, A., Gozani, O., Kutateladze, T. G. and Cleary, M. L. (2010). Binding of the MLL PHD3 finger to histone H3K4me3 is required for MLL-dependent gene transcription. *J. Mol. Biol.* **400**, 137-144.

Chen, J., Santillan, D. A., Koonce, M., Wei, W., Luo, R., Thirman, M. J., Zeleznik-Le, N. J. and Diaz, M. O. (2008). Loss of MLL PHD finger 3 is necessary for MLL-ENL-induced hematopoietic stem cell immortalization. *Cancer Res.* **68**, 6199-6207.

Christensen, J. L. and Weissman, I. L. (2001). Flk-2 is a marker in hematopoietic stem cell differentiation: a simple method to isolate long-term stem cells. *Proc. Natl. Acad. Sci. USA* **98**, 14541-14546.

Crabtree, J. S., Scacheri, P. C., Ward, J. M., Garrett-Beal, L., Emmert-Buck, M. R., Edgemon, K. A., Lorang, D., Libutti, S. K., Chandrasekharappa, S. C., Marx, S. J. et al. (2001). A mouse model of multiple endocrine neoplasia, type 1, develops multiple endocrine tumors. *Proc. Natl. Acad. Sci. USA* **98**, 1118-1123.

Dohda, T., Maljukova, A., Liu, L., Heyman, M., Grander, D., Brodin, D., Sangfelt, O. and Lendahl, U. (2007). Notch signaling induces SKP2 expression and promotes reduction of p27Kip1 in T-cell acute lymphoblastic leukemia cell lines. *Exp. Cell Res.* **313**, 3141-3152.

Donehower, L. A., Harvey, M., Slagle, B. L., McArthur, M. J., Montgomery, C. A., Jr, Butel, J. S. and Bradley, A. (1992). Mice deficient for p53 are developmentally normal but susceptible to spontaneous tumours. *Nature* **356**, 215-221.

Dou, Y., Milne, T. A., Ruthenburg, A. J., Lee, S., Lee, J. W., Verdine, G. L., Allis, C. D. and Roeder, R. G. (2006). Regulation of MLL1 H3K4 methyltransferase activity by its core components. *Nat. Struct. Mol. Biol.* **13**, 713-719.

Ernst, P., Fisher, J. K., Avery, W., Wade, S., Foy, D. and Korsmeyer, S. J. (2004). Definitive hematopoiesis requires the mixed-lineage leukemia gene. *Dev. Cell* **6**, 437-443.

Fair, K., Anderson, M., Bulanova, E., Mi, H., Tropschug, M. and Diaz, M. O. (2001). Protein interactions of the MLL PHD fingers modulate MLL target gene regulation in human cells. *Mol. Cell. Biol.* **21**, 3589-3597.

Ficara, F., Murphy, M. J., Lin, M. and Cleary, M. L. (2008). Pbx1 regulates self-renewal of long-term hematopoietic stem cells by maintaining their quiescence. *Cell Stem Cell* **2**, 484-496.

Forsberg, E. C., Prohaska, S. S., Katzman, S., Heffner, G. C., Stuart, J. M. and Weissman, I. L. (2005). Differential expression of novel potential regulators in hematopoietic stem cells. *PLoS Genet.* **1**, e28.

Franklin, D. S., Godfrey, V. L., Lee, H., Kovalev, G. I., Schoonhoven, R., Chen-Kiang, S., Su, L. and Xiong, Y. (1998). CDK inhibitors p18(INK4c) and p27(Kip1) mediate two separate pathways to collaboratively suppress pituitary tumorigenesis. *Genes Dev.* **12**, 2899-2911.

Franklin, D. S., Godfrey, V. L., O'Brien, D. A., Deng, C. and Xiong, Y. (2000). Functional collaboration between different cyclin-dependent kinase inhibitors suppresses tumor growth with distinct tissue specificity. *Mol. Cell. Biol.* **20**, 6147-6158.

Garcia-Alai, M. M., Allen, M. D., Joerger, A. C. and Bycroft, M. (2010). The structure of the FYR domain of transforming growth factor beta regulator 1. *Protein Sci.* **19**, 1432-1438.

Hess, J. L. (2004). MLL: a histone methyltransferase disrupted in leukemia. *Trends Mol. Med.* **10**, 500-507.

Hsieh, J. J., Cheng, E. H. and Korsmeyer, S. J. (2003a). Taspase1: a threonine aspartase required for cleavage of MLL and proper HOX gene expression. *Cell* **115**, 293-303.

Hsieh, J. J., Ernst, P., Erdjument-Bromage, H., Tempst, P. and Korsmeyer, S. J. (2003b). Proteolytic cleavage of MLL generates a complex of N- and C-terminal fragments that confers protein stability and subnuclear localization. *Mol. Cell. Biol.* **23**, 186-194.

Hughes, C. M., Rozenblatt-Rosen, O., Milne, T. A., Copeland, T. D., Levine, S. S., Lee, J. C., Hayes, D. N., Shanmugam, K. S., Bhattacharjee, A., Biondi, C. A. et al. (2004). Menin associates with a trithorax family histone methyltransferase complex and with the hoxc8 locus. *Mol. Cell* **13**, 587-597.

Jin, S., Zhao, H., Yi, Y., Nakata, Y., Kalota, A. and Gewirtz, A. M. (2010). c-Myb binds MLL through menin in human leukemia cells and is an important driver of MLL-associated leukemogenesis. *J. Clin. Invest.* **120**, 593-606.

Jude, C. D., Climer, L., Xu, D., Artinger, E., Fisher, J. K. and Ernst, P. (2007). Unique and independent roles for MLL in adult hematopoietic stem cells and progenitors. *Cell Stem Cell* **1**, 324-337.

Karnik, S. K., Hughes, C. M., Gu, X., Rozenblatt-Rosen, O., McLean, G. W., Xiong, Y., Meyerson, M. and Kim, S. K. (2005). Menin regulates pancreatic islet growth by promoting histone methylation and expression of genes encoding p27Kip1 and p18INK4c. *Proc. Natl. Acad. Sci. USA* **102**, 14659-14664.

Kim, I., He, S., Yilmaz, O. H., Kiel, M. J. and Morrison, S. J. (2006). Enhanced purification of fetal liver hematopoietic stem cells using SLAM family receptors. *Blood* **108**, 737-744.

Knaevelsrud, H. and Simonsen, A. (2010). Fighting disease by selective autophagy of aggregate-prone proteins. *FEBS Lett.* **584**, 2635-2645.

Kortlever, R. M., Higgins, P. J. and Bernards, R. (2006). Plasminogen activator inhibitor-1 is a critical downstream target of p53 in the induction of replicative senescence. *Nat. Cell Biol.* **8**, 877-884.

Krick, R., Muhe, Y., Prick, T., Bredschneider, M., Bremer, S., Wenzel, D., Eskelinen, E. L. and Thumm, M. (2009). Piecemeal microautophagy of the nucleus: genetic and morphological traits. *Autophagy* **5**, 270-272.

Krivtsov, A. V. and Armstrong, S. A. (2007). MLL translocations, histone modifications and leukaemia stem-cell development. *Nat. Rev. Cancer* **7**, 823-833.

Krivtsov, A. V., Twomey, D., Feng, Z., Stubbs, M. C., Wang, Y., Faber, J., Levine, J. E., Wang, J., Hahn, W. C., Gilliland, D. G. et al. (2006). Transformation from committed progenitor to leukaemia stem cell initiated by MLL-AF9. *Nature* **442**, 818-822.

Kroon, E., Krosl, J., Thorsteinsdottir, U., Baban, S., Buchberg, A. M. and Sauvageau, G. (1998). Hoxa9 transforms primary bone marrow cells through specific collaboration with Meis1a but not Pbx1b. *EMBO J.* **17**, 3714-3725.

Lavau, C., Szilvassy, S. J., Slany, R. and Cleary, M. L. (1997). Immortalization and leukemic transformation of a myelomonocytic precursor by retrovirally transduced HRX-ENL. *EMBO J.* **16**, 4226-4237.

Lawrence, H. J., Christensen, J., Fong, S., Hu, Y. L., Weissman, I., Sauvageau, G., Humphries, R. K. and Largman, C. (2005). Loss of expression of the Hoxa-9

homeobox gene impairs the proliferation and repopulating ability of hematopoietic stem cells. *Blood* **106**, 3988-3994.

Le Toriellec, E., Despouy, G., Pierron, G., Gaye, N., Joiner, M., Bellanger, D., Vincent-Salomon, A. and Stern, M. H. (2008). Haploinsufficiency of CDKN1B contributes to leukemogenesis in T-cell prolymphocytic leukemia. *Blood* **111**, 2321-2328.

Liu, H., Cheng, E. H. and Hsieh, J. J. (2007). Bimodal degradation of MLL by SCFSkp2 and APCCdc20 assures cell cycle execution: a critical regulatory circuit lost in leukemogenic MLL fusions. *Genes Dev.* **21**, 2385-2398.

Löchner, K., Siegler, G., Fuhrer, M., Greil, J., Beck, J. D., Fey, G. H. and Marschalek, R. (1996). A specific deletion in the breakpoint cluster region of the ALL-1 gene is associated with acute lymphoblastic T-cell leukemias. *Cancer Res.* **56**, 2171-2177.

Mansson, R., Hultquist, A., Luc, S., Yang, L., Anderson, K., Kharazi, S., Al-Hashmi, S., Liuba, K., Thoren, L., Adolfsson, J. et al. (2007). Molecular evidence for hierarchical transcriptional lineage priming in fetal and adult stem cells and multipotent progenitors. *Immunity* **26**, 407-419.

Markaki, E. A., Stiakaki, E., Zafiropoulos, A., Arvanitis, D. A., Katzilakis, N., Dimitriou, H., Spandidos, D. A. and Kalmanti, M. (2006). Mutational analysis of the cell cycle inhibitor Kip1/p27 in childhood leukemia. *Pediatr. Blood Cancer.* **47**, 14-21.

McMahon, K. A., Hiew, S. Y., Hadjur, S., Veiga-Fernandes, H., Menzel, U., Price, A. J., Kioussis, D., Williams, O. and Brady, H. J. (2007). Mll has a critical role in fetal and adult hematopoietic stem cell self-renewal. *Cell Stem Cell* **1**, 338-345.

Meyer, C., Kowarz, E., Hofmann, J., Renneville, A., Zuna, J., Trka, J., Ben Abdelali, R., Macintyre, E., De Braekeleer, E., De Braekeleer, M. et al. (2009). New insights to the MLL recombinome of acute leukemias. *Leukemia* **23**, 1490-1499.

Milne, T. A., Briggs, S. D., Brock, H. W., Martin, M. E., Gibbs, D., Allis, C. D. and Hess, J. L. (2002). MLL targets SET domain methyltransferase activity to Hox gene promoters. *Mol. Cell* **10**, 1107-1117.

Milne, T. A., Hughes, C. M., Lloyd, R., Yang, Z., Rozenblatt-Rosen, O., Dou, Y., Schnepp, R. W., Krankel, C., Livolsi, V. A., Gibbs, D. et al. (2005). Menin and MLL cooperatively regulate expression of cyclin-dependent kinase inhibitors. *Proc. Natl. Acad. Sci. USA* **102**, 749-754.

Milne, T. A., Kim, J., Wang, G. G., Stadler, S. C., Basrur, V., Whitcomb, S. J., Wang, Z., Ruthenburg, A. J., Elenitoba-Johnson, K. S., Roeder, R. G. et al. (2010). Multiple interactions recruit MLL1 and MLL1 fusion proteins to the HOXA9 locus in leukemogenesis. *Mol. Cell* **38**, 853-863.

Muntean, A. G., Giannola, D., Udager, A. M. and Hess, J. L. (2008). The PHD fingers of MLL block MLL fusion protein-mediated transformation. *Blood* **112**, 4690-4693.

Muntean, A. G., Tan, J., Sitwala, K., Huang, Y., Bronstein, J., Connelly, J. A., Basrur, V., Elenitoba-Johnson, K. S. and Hess, J. L. (2010). The PAF complex synergizes with MLL fusion proteins at HOX loci to promote leukemogenesis. *Cancer Cell* **17**, 609-621.

Nakamura, T., Mori, T., Tada, S., Krajewski, W., Rozovskaia, T., Wassell, R., Dubois, G., Mazo, A., Croce, C. M. and Canaani, E. (2002). ALL-1 is a histone methyltransferase that assembles a supercomplex of proteins involved in transcriptional regulation. *Mol. Cell* **10**, 1119-1128.

Nam, D. K., Honoki, K., Yu, M. and Yunis, J. J. (1996). Alternative RNA splicing of the MLL gene in normal and malignant cells. *Gene* **178**, 169-175.

Park, Y. E., Hayashi, Y. K., Bonne, G., Arimura, T., Noguchi, S., Nonaka, I. and Nishino, I. (2009). Autophagic degradation of nuclear components in mammalian cells. *Autophagy* **5**, 795-804.

Pless, B., Oehm, C., Knauer, S., Stauber, R. H., Dingermann, T. and Marschalek, R. (2011). The heterodimerization domains of MLL-FYRN and FYRC-are potential target structures in t(4;11) leukemia. *Leukemia* **25**, 663-670.

Sage, J., Mulligan, G. J., Attardi, L. D., Miller, A., Chen, S., Williams, B., Theodorou, E. and Jacks, T. (2000). Targeted disruption of the three Rb-related genes leads to loss of G(1) control and immortalization. *Genes Dev.* **14**, 3037-3050.

Schnabel, C. A., Jacobs, Y. and Cleary, M. L. (2000). HoxA9-mediated immortalization of myeloid progenitors requires functional interactions with TALE cofactors Pbx and Meis. *Oncogene* **19**, 608-616.

Schuettengruber, B., Ganapathi, M., Leblanc, B., Portoso, M., Jaschek, R., Tolhuis, B., van Lohuizen, M., Tanay, A. and Cavalli, G. (2009). Functional anatomy of polycomb and trithorax chromatin landscapes in Drosophila embryos. *PLoS Biol.* **7**, e13.

Silver, P. A., Keegan, L. P. and Ptashne, M. (1984). Amino terminus of the yeast GAL4 gene product is sufficient for nuclear localization. *Proc. Natl. Acad. Sci. USA* **81**, 5951-5955.

Somervaille, T. C. and Cleary, M. L. (2006). Identification and characterization of leukemia stem cells in murine MLL-AF9 acute myeloid leukemia. *Cancer Cell* **10**, 257-268.

Southall, S. M., Wong, P. S., Odho, Z., Roe, S. M. and Wilson, J. R. (2009). Structural basis for the requirement of additional factors for MLL1 SET domain activity and recognition of epigenetic marks. *Mol. Cell* **33**, 181-191.

Steward, M. M., Lee, J. S., O'Donovan, A., Wyatt, M., Bernstein, B. E. and Shilatifard, A. (2006). Molecular regulation of H3K4 trimethylation by ASH2L, a shared subunit of MLL complexes. *Nat. Struct. Mol. Biol.* **13**, 852-854.

Takeuchi, M., Nakaseko, C., Miyagi, S., Takeda, Y., Ozawa, S., Ohwada, C., Cho, R., Nishimura, M., Saito, Y. and Iwama, A. (2008). Clonal expansion of non-leukemic cells expressing two novel MLL-ELL variants differing in transforming activity. *Leukemia* **22**, 861-864.

Thorsteinsdottir, U., Mamo, A., Kroon, E., Jerome, L., Bijl, J., Lawrence, H. J., Humphries, K. and Sauvageau, G. (2002). Overexpression of the myeloid leukemia-associated Hoxa9 gene in bone marrow cells induces stem cell expansion. *Blood* **99**, 121-129.

Wang, Y., Krivtsov, A. V., Sinha, A. U., North, T. E., Goessling, W., Feng, Z., Zon, L. I. and Armstrong, S. A. (2010a). The Wnt/beta-catenin pathway is required for the development of leukemia stem cells in AML. *Science* **327**, 1650-1653.

Wang, Z., Song, J., Milne, T. A., Wang, G. G., Li, H., Allis, C. D. and Patel, D. J. (2010b). Pro isomerization in MLL1 PHD3-bromo cassette connects H3K4me readout to CyP33 and HDAC-mediated repression. *Cell* **141**, 1183-1194.

Yagi, H., Deguchi, K., Aono, A., Tani, Y., Kishimoto, T. and Komori, T. (1998). Growth disturbance in fetal liver hematopoiesis of Mll-mutant mice. *Blood* **92**, 108-117.

Yokoyama, A. and Cleary, M. L. (2008). Menin critically links MLL proteins with LEDGF on cancer-associated target genes. *Cancer Cell* **14**, 36-46.

Yokoyama, A., Kitabayashi, I., Ayton, P. M., Cleary, M. L. and Ohki, M. (2002). Leukemia proto-oncoprotein MLL is proteolytically processed into 2 fragments with opposite transcriptional properties. *Blood* **100**, 3710-3718.

Yokoyama, A., Wang, Z., Wysocka, J., Sanyal, M., Aufiero, D. J., Kitabayashi, I., Herr, W. and Cleary, M. L. (2004). Leukemia proto-oncoprotein MLL forms a SET1-like histone methyltransferase complex with menin to regulate Hox gene expression. *Mol. Cell. Biol.* **24**, 5639-5649.

Yokoyama, A., Somervaille, T. C., Smith, K. S., Rozenblatt-Rosen, O., Meyerson, M. and Cleary, M. L. (2005). The menin tumor suppressor protein is an essential oncogenic cofactor for MLL-associated leukemogenesis. *Cell* **123**, 207-218.

Yu, B. D., Hess, J. L., Horning, S. E., Brown, G. A. and Korsmeyer, S. J. (1995). Altered Hox expression and segmental identity in Mll-mutant mice. *Nature* **378**, 505-508.

Yu, B. D., Hanson, R. D., Hess, J. L., Horning, S. E. and Korsmeyer, S. J. (1998). MLL, a mammalian trithorax-group gene, functions as a transcriptional maintenance factor in morphogenesis. *Proc. Natl. Acad. Sci. USA* **95**, 10632-10636.

Zeleznik-Le, N. J., Harden, A. M. and Rowley, J. D. (1994). 11q23 translocations split the "AT-hook" cruciform DNA-binding region and the transcriptional repression domain from the activation domain of the mixed-lineage leukemia (MLL) gene. *Proc. Natl. Acad. Sci. USA* **91**, 10610-10614.

Journal of Cell Science

blood

2011 118: 2443-2453
Prepublished online July 13, 2011;
doi:10.1182/blood-2011-01-331892

The Hbo1-Brd1/Brpf2 complex is responsible for global acetylation of H3K14 and required for fetal liver erythropoiesis

Yuta Mishima, Satoru Miyagi, Atsunori Saraya, Masamitsu Negishi, Mitsuhiro Endoh, Takaho A. Endo, Tetsuro Toyoda, Jun Shinga, Takuo Katsumoto, Tetsuhiro Chiba, Naoto Yamaguchi, Issay Kitabayashi, Haruhiko Koseki and Atsushi Iwama

Blood (print ISSN 0006-4971, online ISSN 1528-0020), is published weekly by the American Society of Hematology, 2021 L St, NW, Suite 900, Washington DC 20036.

The Hbo1-Brd1/Brpf2 complex is responsible for global acetylation of H3K14 and required for fetal liver erythropoiesis

*Yuta Mishima,[1-3] *Satoru Miyagi,[1,3] *Atsunori Saraya,[1,3] Masamitsu Negishi,[1,3] Mitsuhiro Endoh,[3,4] Takaho A. Endo,[5] Tetsuro Toyoda,[5] Jun Shinga,[4] Takuo Katsumoto,[6] Tetsuhiro Chiba,[1,3] Naoto Yamaguchi,[2] Issay Kitabayashi,[6] Haruhiko Koseki,[3,4] and Atsushi Iwama[1,3]

[1]Department of Cellular and Molecular Medicine, Graduate School of Medicine, and [2]Department of Molecular Cell Biology, Graduate School of Pharmaceutical Sciences, Chiba University, Chiba, Japan; [3]JST, CREST, Tokyo, Japan; [4]RIKEN Research Center for Allergy and Immunology, Yokohama, Japan; [5]RIKEN Genomic Sciences Center, Yokohama, Japan; and [6]Molecular Oncology Division, National Cancer Center Research Institute, Tokyo, Japan

The histone acetyltransferases (HATs) of the MYST family include TIP60, HBO1, MOZ/MORF, and MOF and function in multisubunit protein complexes. Bromodomain-containing protein 1 (BRD1), also known as BRPF2, has been considered a subunit of the MOZ/MORF H3 HAT complex based on analogy with BRPF1 and BRPF3. However, its physiologic function remains obscure. Here we show that BRD1 forms a novel HAT complex with HBO1 and regulates erythropoiesis. *Brd1*-deficient embryos showed severe anemia because of impaired fetal liver erythropoiesis. Biochemical analyses revealed that BRD1 bridges HBO1 and its activator protein, ING4. Genome-wide mapping in erythroblasts demonstrated that BRD1 and HBO1 largely colocalize in the genome and target key developmental regulator genes. Of note, levels of global acetylation of histone H3 at lysine 14 (H3K14) were profoundly decreased in *Brd1*-deficient erythroblasts and depletion of Hbo1 similarly affected H3K14 acetylation. Impaired erythropoiesis in the absence of Brd1 accompanied reduced expression of key erythroid regulator genes, including *Gata1*, and was partially restored by forced expression of *Gata1*. Our findings suggest that the Hbo1-Brd1 complex is the major H3K14 HAT required for transcriptional activation of erythroid developmental regulator genes. (*Blood*. 2011;118(9):2443-2453)

Introduction

The histone acetyltransferases (HATs) of the MYST family, which include TIP60, HBO1, MOZ/MORF, and MOF, are highly conserved in eukaryotes and perform a significant proportion of all nuclear acetylation. They share a highly conserved MYST domain composed of an acetyl-CoA binding motif and a zinc finger and function in multisubunit protein complexes.[1,2] Among the MYST family members, HBO1 and MOZ/MORF form complexes of very similar composition: JADE family proteins bridge HBO1 with inhibitor of growth 4 and 5 (ING4/5) and Esa1-associated factor 6 ortholog (EAF6), whereas BRPF family proteins bridge MOZ/MORF with ING5 and EAF6, respectively.[1,3,4] The plant homology domain (PHD) fingers in JADE1/2/3, BRPF1/2/3, and ING4/5 interact with histones and are thought to define the substrate-specificity of the HBO1 and MOZ/MORF complexes.[1] HBO1 is considered responsible for the bulk of the acetylation of histone H4 at lysines 5, 8, and 12 (H4K5, K8, and K12), and the interaction between ING4 and histone H3 trimethylated at lysine 4 (H3K4me3) augments activity of HBO1 to acetylate histone H3.[5] Furthermore, the HBO1 complexes are enriched throughout the coding regions of genes, suggestive of a role in transcriptional elongation.[6] By contrast, MOZ and MORF are HATs specific for histone H3. Binding of Yng1, a yeast ortholog of the ING family, to H3K4me3 has been shown to promote Sas3 (yeast ortholog of MOZ) HAT activity at H3K14.[7] The mammalian MOZ complex also showed specificity for H3K14 acetylation in vitro.[3]

Moz-deficient mice have a severe defect in the maintenance of HSCs.[8,9] During zebrafish development, both *moz* and *brpf1* are required for maintenance of cranial *Hox* gene expression and proper determination of pharyngeal segmental identities.[10,11] Similar findings were reported from analyses of *Moz*-deficient mice and medaka fish in which *brpf1* was mutated.[12] The genetic interaction between *Moz* and *Brpf1* supports that Brpf1 is the major bridging protein of the MOZ HAT complex. In contrast to Brpf1, however, distinctive functions of other BRPF family members have not been elucidated.

BRD1 (initially named BR140-LIKE; BRL) was originally cloned as a protein containing a cysteine-rich region related to that of AF10 and AF17, which are leukemic fusion partners of MLL.[13] BRD1 contains a bromodomain, 2 PHD zinc fingers, and a proline-tryptophan-tryptophan-proline (PWWP) domain, 3 types of modules characteristic of chromatin regulators. Recently, BRD1 was reported to belong to a small family of BRPF proteins that includes BRPF1, BRD1/BRPF2, and BRPF3.[1,3] BRD1 has been considered a subunit of the MOZ/MORF H3 HAT complex on the basis of analogy with BRPF1 and BRPF3.[3,4] However, no detailed analysis of BRD1 has been reported. In this study, we found that BRD1 forms a novel HAT complex with HBO1 and is responsible for the bulk of the acetylation of H3K14. We confirmed a drastic reduction in levels of acetylated H3K14 in *Brd1*-deficient mice and found that the Hbo1-Brd1 HAT complex is required for full

Submitted January 20, 2011; accepted June 20, 2011. Prepublished online as *Blood* First Edition paper, July 13, 2011; DOI 10.1182/blood-2011-01-331892.

*Y.M., S.M., and A.S. contributed equally to this work.

The online version of this article contains a data supplement.

The publication costs of this article were defrayed in part by page charge payment. Therefore, and solely to indicate this fact, this article is hereby marked "advertisement" in accordance with 18 USC section 1734.

transcriptional activation of the erythroid-specific regulator genes essential for terminal differentiation and survival of erythroblasts in fetal liver.

Methods

Gene targeting of *Brd1*

Brd1-deficient mice were generated by the use of R1 embryonic stem cells according to the conventional protocol. *Brd1*-deficient mice were backcrossed to the C57BL/6 background > 5 times. All experiments in which mice were used received approval from the Chiba University Administrative Panel for Animal Care.

Viral production

To prepare the retrovirus, pMC-ires-GFP was used as a vector.[14] The production and concentration of the recombinant retrovirus have been described previously.[15] To prepare the lentivirus, pCSII-EF1-MCS-IRESII-Venus and pCS-H1-shRNA-EF-1α-EGFP were used as vectors.[16] The viruses were produced as described previously.[16] Target sequences were as follows; Sh-*mHbo1*#2; GAGGGAAGCAACATGATTA, Sh-*mHbo1*#3; GTGATGAGATTTATCGCAA, Sh-*hHBO1*#1; GGGATAAGCAGATAGAAGA, and Sh-*hHBO1*#3; CTCAAATACTGGAAGGGAA.

Purification of BRD1-containing protein complex

Protein purification, trypsin digestion, and liquid chromatography tandem mass spectrometry (LC/MS/MS) were performed as described previously.[17] In brief, K562 cells expressing Flag-Brd1 (2.5×10^8 cells) were suspended in 15 mL of lysis buffer (20mM sodium phosphate, pH 7.0; 350mM NaCl; 30mM sodium pyrophosphate; 0.1% NP-40; 5mM EDTA; 10mM NaF; 0.1mM Na_3VO_4; and 1mM phenylmethylsulfonyl fluoride) containing protease inhibitors (cOmplete mini; Roche) and sonicated for 20 minutes. The lysates were cleared by centrifugation and incubated with 100 μL of anti-FLAG M2 affinity gel (Sigma-Aldirch) with rotation at 4°C for 16 hours. The beads were extensively washed 6 times with 15 mL of lysis buffer. The complexes were eluted by incubating twice with 0.2 mg/mL of FLAG peptide in 300 μL of lysis buffer for 2.5 hours. This purification was repeated 10 times. Then, eluents were pooled and concentrated by the use of a filtration device (Vivaspin 10K-PES; Sartorius) and separated by 7.5%-15% SDS-PAGE.

Immunoprecipitation and extraction of histones

Transfected 293T cells were lysed in lysis buffer containing 250mM NaCl and then immunoprecipitation was performed. Immunocomplexes were eluted with FLAG peptide as describe previously. Histone proteins were extracted following the method described previously.[18]

ChIP-on-chip experiment

ChIP-on-chip analyses of BRD1 and HBO1 binding were performed by use of the Human Promoter ChIP-on-chip Microarray Set (G4489A; Agilent Technologies). The assignment of IP regions and calculations were performed as described.[19] K562 cells were fixed with 1% formaldehyde in PBS for 10 minutes at room temperature and washed twice with PBS. Fixed cells swelled in the buffer (20mM HEPES, pH 7.8; 1.5mM $MgCl_2$; 10mM KCl; 0.1% NP-40; and 1mM DTT) for 10 minutes on ice and nuclei were prepared by Dounce homogenizer. Nuclei were then lysed with RIPA (10mM Tris, pH 8.0; 0.5% SDS; 140mM NaCl; 1mM EDTA; 1% TritonX-100; 0.1% SDS; 0.1% sodium deoxycholate; and a proteinase inhibitor cocktail [cOmplete mini]), and sonicated for 30 minutes with a Bioruptor (Cosmobio Co Ltd). After centrifugation, the soluble chromatin fraction was precleared with a mixture of protein A and G-conjugated Dynabeads (Invitrogen) blocked with BSA and salmon sperm DNA. Three hundred micrograms of chromatin was immunoprecipitated overnight at 4°C with the use of 25 μL of antibody-conjugated Dynabeads. The immunoprecipitates were washed extensively and subjected to a quantitative PCR analysis with SYBR Premix Ex TaqTM II (Takara). For the ChIP of erythroblasts, the steps to prepare nuclei were omitted, and fixed cells were directly lysed by RIPA. Primer sequences used are listed in supplemental Methods (available on the *Blood* Web site; see the Supplemental Materials link at the top of the online article).

Expression vectors and antibodies

Other methods, the expression vectors, and antibodies used are described in supplemental Methods.

Results

Brd1$^{-/-}$ embryos die at mid-gestation because of anemia

To clarify the physiologic function of Brd1, we generated *Brd1*-deficient mice in which exon 2 containing the first ATG of the *Brd1* gene was deleted (Figure 1A). Northern blot analysis detected no *Brd1* mRNA in *Brd1*$^{-/-}$ embryos (data not shown). The *Brd1*$^{-/-}$ embryos were recovered at nearly the expected Mendelian ratio at 12.5 days postcoitum (dpc) but most had died by 15.5 dpc (Table 1). *Brd1*$^{-/-}$ embryos showed growth retardation (92 of 99 embryos at 12.5 dpc), failure to fuse the neural tube (30 of 135 embryos at 8.5-12.5 dpc), and abnormal lenses with disoriented optic cups (74 of 122 embryos at 10.5-12.5 dpc; Figure 1B and Table 1). These results indicated Brd1 as having pivotal roles in embryonic development in multiple tissues and organs, but none of them was considered to be the cause of death.

We then analyzed hematopoiesis in the absence of Brd1. Numbers of total yolk sac cells and Ter119$^+$ erythroblasts were rather increased in *Brd1*$^{-/-}$ yolk sac compared with those in wild-type yolk sac (Figure 1C-D). This trend was more apparent at later stages. At 12.5 dpc, erythropoiesis was still active in *Brd1*$^{-/-}$ yolk sac, whereas erythropoiesis tended to decline in wild-type yolk sac (supplemental Figure 1A). Together, our findings suggest that primitive erythropoiesis in the *Brd1*$^{-/-}$ yolk sac was not affected but rather enhanced. Nevertheless, *Brd1*$^{-/-}$ embryos at 12.5 dpc were pale and the fetal liver, in which fetal hematopoiesis mainly occurs, was significantly smaller than that of littermate controls (Figure 2A-D). Cytologic analysis revealed that *Brd1*$^{-/-}$ fetal livers had profoundly fewer erythroblasts beyond the proerythroblast stage than did wild-type fetal livers (Figure 2E-F).

Brd1 is required for erythropoiesis in fetal liver

Among the phenotypes associated with *Brd1* deficiency, we focused on anemia, which is a major causative defect for lethality at this stage of development. Flow cytometric analysis of fetal livers at 12.5 dpc revealed a 2-fold reduction in the Ter119$^+$ erythroid cell fraction and a 2-fold increase in the c-Kit$^+$ hematopoietic progenitor fraction (Figure 2G). Because the total number of *Brd1*$^{-/-}$ fetal liver cells was decreased to 22% of the control, the absolute number of Ter119$^+$ erythroid cells was decreased by 91% in *Brd1*$^{-/-}$ fetal livers compared with wild-type fetal livers, whereas that of c-Kit$^+$ hematopoietic progenitors was not profoundly changed (Figure 2H). The number of Dlk1$^+$ hepatoblasts was reduced to 57% of the control, but the differentiation of hepatoblasts into hepatocytes and cholangiocytes was grossly normal in the *Brd1*$^{-/-}$ fetal liver (Figure 2G-H; and data not shown). These results indicated that the fetal liver hypoplasia in *Brd1*$^{-/-}$ embryos was mainly caused by a reduction in numbers of erythroid lineage cells.

Detailed flow cytometric analyses revealed a significant increase in the CD71$^+$Ter119$^-$ fraction and a drastic reduction in the

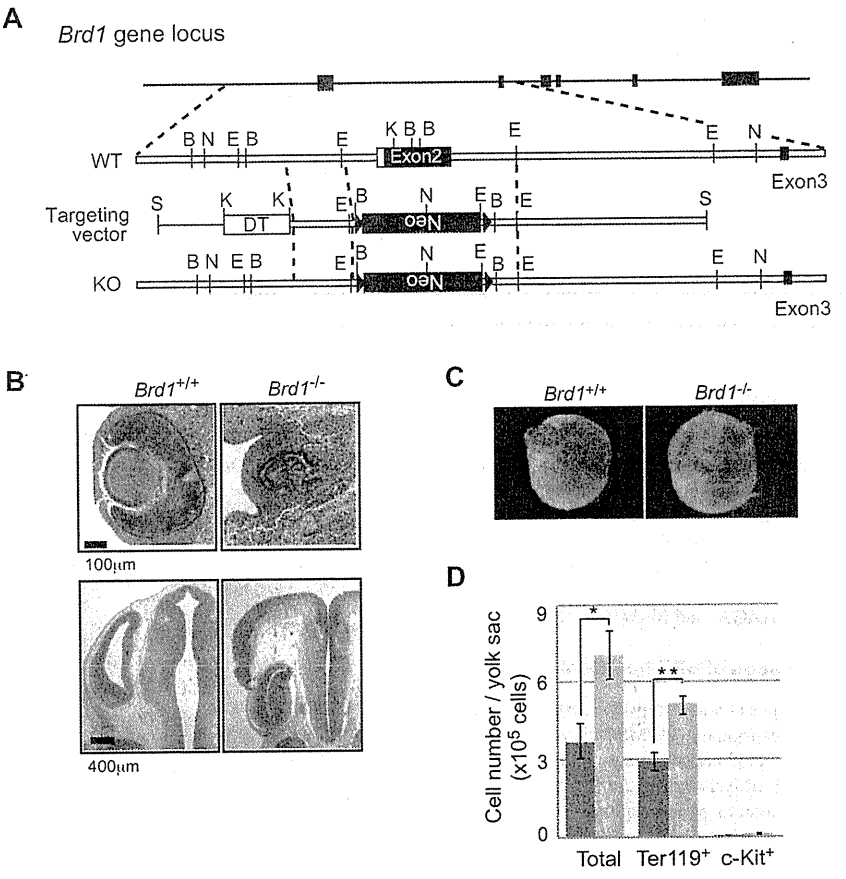

Figure 1. Targeted disruption of the mouse *Brd1* gene. (A) Strategy for making a knockout allele for *Brd1* by homologous recombination in ES cells. B, *Bam*HI; N, *Nco*I; E, *Eco*RI; K, *Kpn*I; S, *Sal*I. (B) Developmental defects in *Brd1*$^{-/-}$ embryos. Abnormal lenses with disoriented optic cups (top) and neural tube disclosure (bottom) in *Brd1*$^{-/-}$ embryos at 12.5 dpc. Sections were stained with hematoxylin and eosin. (C) Appearance of wild-type (*Brd1*$^{+/+}$, left) and *Brd1*$^{-/-}$ (right) yolk sac at 10.5 dpc. (D) Absolute numbers of total cells, c-Kit^{+} hematopoietic progenitors, and Ter119^{+} erythroid cells in 10.5 dpc yolk sac from wild-type (left bar, n = 5) and *Brd1*$^{-/-}$ (right bar, n = 3) embryos. The results are shown as the mean ± SE $^{*}P < .05$, $^{**}P < .005$.

CD71^{+}Ter119^{+} and CD71^{-}Ter119^{+} fractions in *Brd1*$^{-/-}$ fetal livers compared with wild-type fetal livers (Figure 2I-J). The CD45^{-}c-Kit^{+}CD71^{+}Ter119^{-} CFU-erythroid fraction was also more prevalent in *Brd1*$^{-/-}$ fetal livers (Figure 2J top). These results indicate a differentiation block of *Brd1*$^{-/-}$ fetal liver erythroblasts at the transition from CD71^{+}Ter119^{-} to CD71^{+}Ter119^{+} stage. Nonetheless, absolute numbers of cells in each fraction, particularly the CD71^{+}Ter119^{+} and CD71^{-}Ter119^{+} fractions, were significantly decreased (Figure 2J bottom). To further elucidate the mechanism by which *Brd1* deficiency causes defective erythropoiesis, we examined the apoptosis of erythroblasts. Apoptotic cells with an active caspase-3 were readily detected in *Brd1*$^{-/-}$ fetal livers (supplemental Figure 1B). The number of annexin V^{+}/7-aminoactinomycin D^{-} apoptotic cells was also significantly elevated in *Brd1*$^{-/-}$ fetal livers; cell death was even further exacerbated in the CD71^{+}Ter119^{+} and CD71^{-}Ter119^{+} fractions (Figure 2K). Thus, loss of Brd1 in fetal liver erythroblasts causes massive apoptosis and maturation delay, leading to severe anemia. These findings suggested that severe anemia combined with other physiologic defects accounts for the death of *Brd1*$^{-/-}$ embryos.

Table 1. Analysis of *Brd1*-heterozygous intercross progenies

Stage, dpc	*Brd1*$^{+/+}$	*Brd1*$^{+/-}$	*Brd1*$^{-/-}$	ND	Total progenies
8.5-9.5	5	20	13 (1)*†	3	41
10.5-11.5	24	49	23 (2)‡§¶	5	101
12.5	117	238 (2)	99 (4)#‖**	44	498
13.5	10	15	2††	1	28
14.5-15.5	4	22	1	6	23
16.5-18.5	3	4	0	13	20
Weaning	17	23	0	0	40

Numbers in parentheses indicate dead embryos.
dpc indicates days postcoitum; and ND, not determined.
*Six embryos showed growth retardation.
†Four embryos showed failure to fuse the neural tube.
‡Twenty-one embryos showed growth retardation.
§Two embryos showed failure to fuse the neural tube.
¶Three embryos showed abnormal eye development.
#Ninety-two embryos showed growth retardation.
‖Twenty-four embryos showed failure to fuse the neural tube.
**Seventy-one embryos showed abnormal eye development.
††One embryo showed abnormal eye development.

BRD1 forms an active HAT complex with HBO1 and ING4

Analogous to BRPF1, BRD1/BRPF2 has been proposed to form a H3 HAT complex with MOZ.[3,4] Similar to *Brd1*$^{-/-}$ mice, *Moz*$^{-/-}$ mice die in the embryonic stage and show impaired fetal liver hematopoiesis. However, the hematopoietic defect in *Moz*$^{-/-}$ fetal livers is observed mainly in HSCs.[8,9] To address this discrepancy, we purified BRD1-containing protein complexes by Flag epitope-specific immune-affinity purification from K562 human leukemic cells expressing Flag-BRD1 and analyzed them by LC/MS/MS (Figure 3A). The LC/MS/MS analysis identified several proteins as putative components of the BRD1 complex. Among these proteins, we focused on ING4 and HBO1 because HBO1 and ING4 were reproducibly and substoichiometrically copurified with Flag-BRD1 in our repeated purifications. Immunoblotting of the purified fraction confirmed the presence of HBO1 and ING4 in the complex (Figure 3B). HBO1 and MOZ have been demonstrated to form similar protein complexes with ING4/5, JADE1/2/3, and hEAF6 and ING5, BRPF1/2/3, and hEAF6, respectively, in HeLa cells.[1,2]

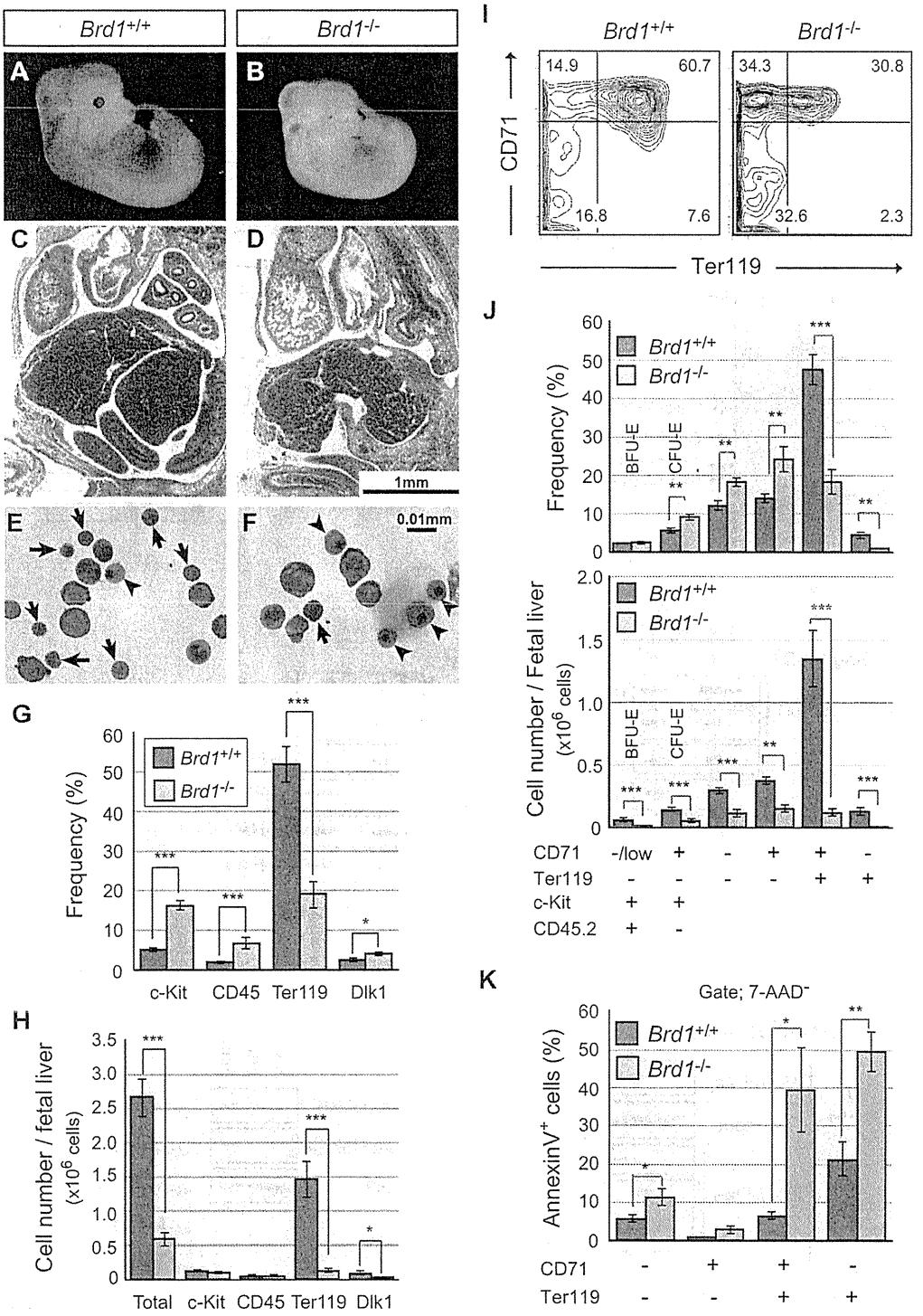

Figure 2. Impaired hematopoiesis in *Brd1*$^{-/-}$ fetal liver. Appearance of wild-type (A) and *Brd1*$^{-/-}$ (B) embryos at 12.5 dpc. H&E-stained transverse sections of 12.5 dpc wild-type (C) and *Brd1*$^{-/-}$ (D) embryos. Morphology of 12.5 dpc fetal liver hematopoietic cells from wild-type (E) and *Brd1*$^{-/-}$ (F) embryos stained with May-Grüenwald-Giemsa solutions. Arrows and arrowheads indicate mature erythroblasts and nucleated erythrocytes, respectively. Frequency (G) and absolute cell numbers (H) of c-Kit$^+$ hematopoietic progenitors, CD45$^+$ hematopoietic cells, Ter119$^+$ erythroid cells, and Dlk1$^+$ hepatoblasts in 12.5 dpc fetal livers from wild-type and *Brd1*$^{-/-}$ embryos. The results are shown as the mean ± SE (n ≥ 4). $^*P < .05$, $^{***}P < .0005$. (I) Flow cytometric profiles of erythroid differentiation defined by CD71 and Ter119 expression in representative fetal livers at 12.5 dpc. The percentage of each fraction is indicated. (J) Frequency (top) and absolute cell numbers (bottom) of BFU-E, CFU-erythroid, CD71$^-$Ter119$^-$ cells, CD71$^+$Ter119$^-$ erythroblasts, CD71$^+$Ter119$^+$ erythroblasts, and CD71$^-$Ter119$^+$ erythroblasts in 12.5 dpc fetal livers from wild-type and *Brd1*$^{-/-}$ embryos. The results are shown as the mean ± SE (n ≥ 8). $^{**}P < .005$, $^{***}P < .0005$. (K) Massive apoptosis of *Brd1*$^{-/-}$ erythroblasts. The percentage of annexin V$^+$/7-aminoactinomycin D$^-$ (7-AAD$^-$) apoptotic cells in each fraction defined by CD71 and Ter119 is shown as the mean ± SE (n ≥ 4). $^*P < .05$, $^{**}P < .005$.

JADE and BRPF family proteins function as a bridging protein between HBO1 and ING4/5 and MOZ and ING5, respectively.

To determine the physical interaction among HBO1, BRD1, and ING4 in the complex, we transfected 293T cells with different

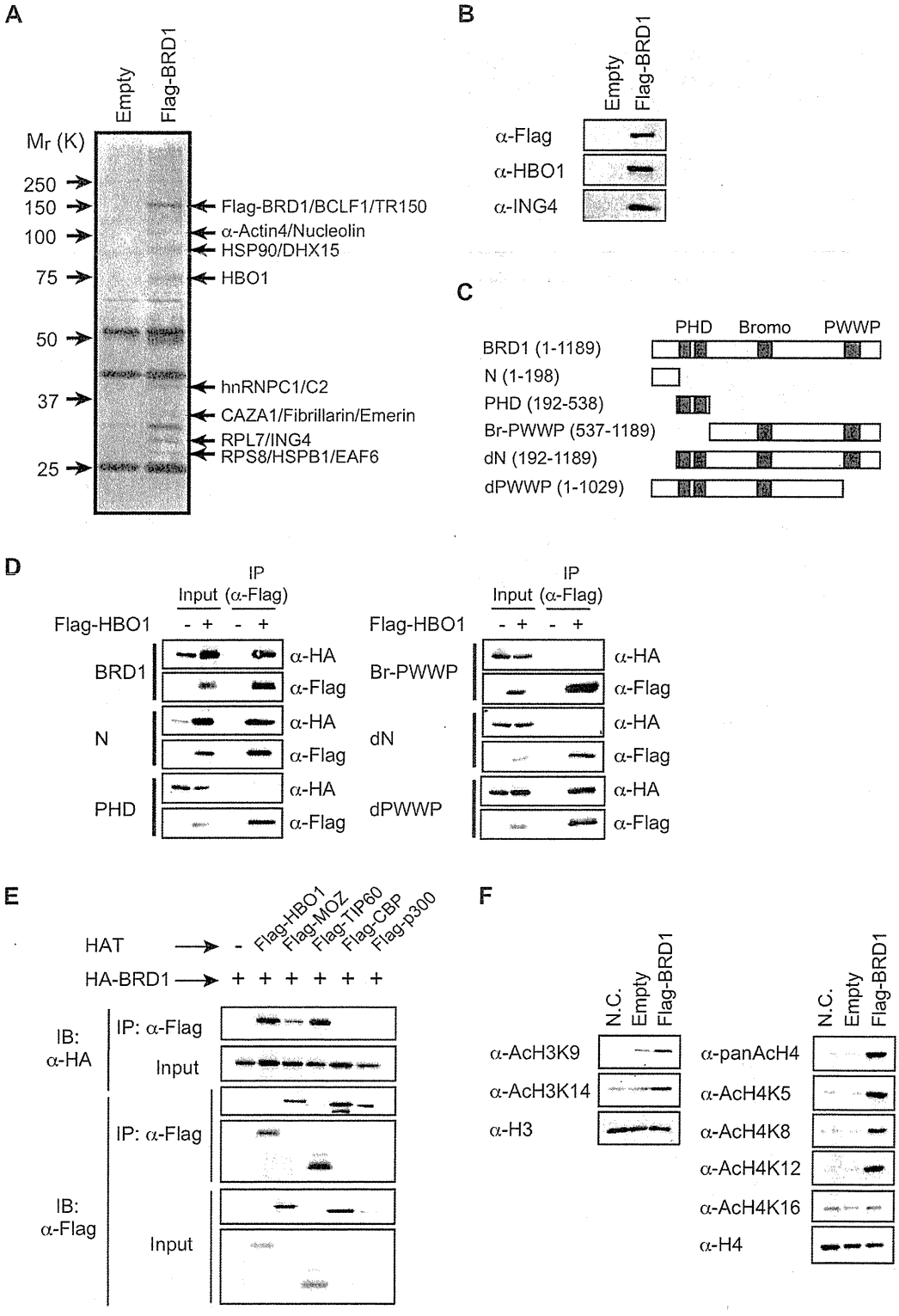

Figure 3. BRD1 forms a HAT complex with HBO1. (A) Purification of the BRD1 complex. Flag-tagged BRD1 protein was partially purified from lysates of K562/Flag-BRD1 cells using an anti-Flag antibody. (B) Western blot analysis of the purified BRD1 complex in panel A by the use of indicated antibodies. (C) Schematic representation of BRD1 and its deletion mutants. Three major domains are indicated. (D) Localization of the binding site in BRD1 for HBO1. 293T cells were transfected with HA-tagged BRD1 mutants with and without Flag-tagged HBO1. Proteins in the lysates of the transfectants were immunoprecipitated with the anti-FLAG antibody and eluted with an excess of Flag peptide. The eluents were analyzed by Western blotting by the use of anti-Flag or HA antibodies. (E) Affinity of BRD1 for the MYST family HATs (HBO1, MOZ, and Tip60) and CBP/p300. 293T cells were transfected with HA-tagged Brd1 together with indicated Flag-tagged HATs. Proteins in the lysates of the transfectants were immunoprecipitated with the anti-FLAG antibody. The immunoprecipitates were analyzed by Western blotting with anti-Flag and HA antibodies. (F) HAT activity of the BRD1 complex. The BRD1 complex was partially purified from lysates of K562/empty vector (Empty) and K562/Flag-BRD1 cells by the use of the anti-Flag antibody and HAT activity on recombinant histones H3 and H4 was evaluated. As a negative control (N.C.), the recombinant histones H3 and H4 were similarly treated without HAT complexes.

combinations of *BRD1*, *HBO1*, and *ING4*. HBO1 and ING4 were coimmunoprecipitated only in the presence of BRD1, whereas BRD1 was coimmunoprecipitated with HBO1 or ING4 in the absence of ING4 and HBO1, respectively (supplemental Figure 2A-C). These results indicate that BRD1 functions as a scaffold to link HBO1 with ING4 and form a ternary complex. To confirm the formation of a complex between the endogenous Brd1 and Hbo1 proteins, we immunoprecipitated Brd1 with an anti-Brd1 antibody from both wild-type and *Brd1*$^{-/-}$ whole embryos at 12.5 dpc. Of note, Hbo1 was detected in the immunoprecipitates from wild-type but not *Brd1*$^{-/-}$ embryos (supplemental Figure 2E).

The Brd1 mutants containing the N-terminal 198 amino acids (N and dPWWP) interacted with HBO1, whereas fragments lacking the N-terminal 192 amino acids did not (PHD, Br-PWWP, and dN; (Figure 3C-D). These results indicate that the N-terminal 198 amino acids of BRD1 are necessary and sufficient for physical interaction with HBO1. Conversely, the BRD1-interacting domain was localized to the MYST domain of HBO1 (supplemental Figure 2D). We then tested whether the complementation of *Brd1*$^{-/-}$ progenitors with exogenous *Brd1* can rescue their compromised erythroid differentiation in vitro. We purified c-Kit^{+}CD71^{-} hematopoietic progenitors from 12.5 dpc fetal livers. The cells were retrovirally transduced with the wild-type *Brd1* or dN mutant and then cultured for 3 days in the presence of erythropoietin (EPO) to induce erythroid differentiation (supplemental Figure 3). As expected, wild-type *Brd1* but not dN mutant considerably canceled the differentiation block of *Brd1*$^{-/-}$ erythroblasts at the transition from CD71^{+}Ter119^{-} to CD71^{+}Ter119^{+} stage. These results further support the formation of a complex between BRD1 and HBO1 through the N terminus of Brd1.

We also noted that coexpression of HBO1 increases the protein level of BRD1 (Figure 3D; see inputs of BRD1, N, and dPWWP) in 293T cells. The treatment of the cells with MG132, a proteasome inhibitor, also increased the BRD1 protein level, strongly suggesting that HBO1 stabilizes the BRD1 protein by inhibiting the proteasome-dependent protein degradation pathway (supplemental Figure 4A). Similar levels of protein stabilization were observed when HBO1 was coexpressed with BRD1 deletions retaining an HBO1-binding capacity, but not dN, which lacked the HBO1-binding domain (supplemental Figure 4A), indicating that the N-terminal 198 amino acids are required not only for BRD1-HBO1 interaction but also for stability of the BRD1 protein. These findings further support the formation of a complex between BRD1 and HBO1.

We then examined the interaction of BRD1 with various HATs. Coimmunoprecipitation assays demonstrated that BRD1 binds mainly to HBO1 and TIP60, moderately to MOZ, and not at all to CBP and p300 (Figure 3E). In contrast, BRPF1 preferred MOZ and bound moderately to HBO1 (supplemental Figure 4B). The difference in affinity for HATs between BRD1 and BRPF1 was evident when they were forced to compete with each other to form complexes. This experiment clearly showed that BRD1 and BRPF1 prefer to bind with HBO1 and MOZ, respectively (supplemental Figure 4C).

The HBO1 HAT complex is reportedly responsible for the bulk of the acetylation of H4K5, K8, and K12 and also acetylates histone H3.[3,5,20] The BRD1 complex from K562 cells efficiently acetylated the recombinant histone H4 at K5, K8, and K12, but not K16, and moderately acetylated the recombinant histone H3 at K9 and 14 (Figure 3F). These findings implied that BRD1 and HBO1 form a novel HAT complex that differs in composition from known HAT complexes.

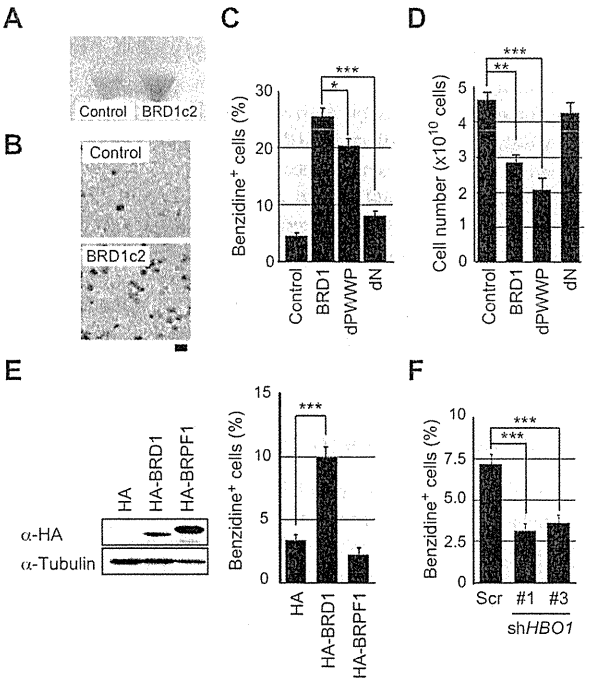

Figure 4. Overexpression of BRD1 induces erythroid differentiation in K562. (A) Appearance of parental K562 cells (Control) and the Flag-BRD1-expressing clone (BRD1c2) used for purification of the BRD1 complex. (B) Benzidine staining of parental K562 cells (Control) and Brd1c2. The bar indicates 20 μm (C) Benzidine staining of K562 cells expressing BRD1 mutants. K562 cells were transduced with an empty vector (Control) or retroviruses expressing full-length BRD1 (BRD1), dPWWP, or dN. Transduced cells were sorted with the use of GFP as a marker antigen and expanded for benzidine staining. Bars represent mean ± SE (n = 12). (D) Growth of K562 cells expressing BRD1 or the BRD1 mutant in (C). The results are shown as the mean ± SE for triplicate cultures. (E) Overexpression of BRPF1 in K562 cells. K562 cells were transduced with a HA-BRPF1 retrovirus, and BRPF1 expression was detected by Western blotting by use of the anti-HA antibody (left). Effects of BRPF1 on erythroid differentiation of K562 cells were evaluated by benzidine staining. The data are shown as the mean ± SE for triplicate cultures. (F) Knockdown of *HBO1* with the use of shRNA. K562 cells were infected with lentiviruses expressing shRNAs against *HBO1* and analyzed as to the basal status of hemoglobinization by benzidine staining. The results are shown as the mean ± SE for triplicate cultures. $^{*}P < .05$, $^{**}P < .005$, $^{***}P < .0005$.

The HBO1-BRD1 complex promotes erythroid differentiation

K562 human leukemic cells, which we used for purification of the BRD1 complex, have a potential to differentiate along the erythroid lineage. We found that overexpression of BRD1 promotes hemoglobinization of K562 cells (clone BRD1c2, Figure 4A). Enhanced hemoglobin production was confirmed by benzidine staining in BRD1c2 (Figure 4B, benzidine-positive cells, control cells 5.3% ± 0.4% vs BRD1c2 18.4% ± 0.3%) and in a series of other clones (supplemental Figure 5A-B, control cells 5.7% ± 2.3% vs Flag-BRD1 25.6% ± 6.7%). Expression of glycophorin A, an erythroid lineage marker antigen, on the cell surface, was also significantly increased in the BRD1-overexpressing clones (supplemental Figure 5C-D, control cells 29.0% ± 0.3% vs Flag-BRD1 72.0% ± 0.2%). These results indicated that BRD1 induces erythroid differentiation of K562 cells.

To understand the mechanism of the BRD1-mediated erythroid differentiation, we examined the impact of BRD1 deletions on erythroid differentiation of K562 cells. The capacity of BRD1 to induce erythroid differentiation was profoundly affected by deletion of the N-terminus, which mediates interaction with HBO1 (dN mutant; Figure 4C), although the dN mutant was expressed and localized to the nucleus (data not shown). In contrast, the C-terminal deletion mutant (dPWWP) still

had a significant effect (Figure 4C). Both BRD1 and dPWWP significantly reduced cell growth probably as a consequence of erythroid differentiation (Figure 4D). These results indicate that the HBO1-binding domain is indispensable for BRD1 to induce erythroid differentiation. We also tested the effect of BRPF1, which mostly binds to MOZ, and found that BRPF1 does not induce erythroid differentiation (Figure 4E), implying that the HBO1-BRD1 complex has a distinct function from the MOZ-BRPF1 complex in erythroid cells. We then examined whether HBO1 has a significant impact on erythroid differentiation by knocking down its expression. We transduced K562 cells with lentiviruses expressing shRNA against the human HBO1 (sh*HBO1*#1 and #3) and a scrambled control shRNA sequence. The percentages of benzidine$^+$ cells were significantly reduced by *HBO1* knockdown even in uninduced K562 cells (Figure 4F).

Localization of the HBO1-BRD1 complex in the human genome

To identify the direct target genes of the HBO1-BRD1 complex, we conducted a ChIP-on-chip analysis in K562 cells coexpressing 3xFlag-BRD1 and HA-HBO1, and we identified 2120 and 1852 genes bound by BRD1 and HBO1, respectively (full data are listed in supplemental ChIP-chip dataset). Of these, 1379 genes were co-occupied by BRD1 and HBO1, indicating that BRD1 and HBO1 coregulate a significant portion of their target genes in erythroid cells (Figure 5A). The peaks of BRD1 and HBO1 signals coincided around −1.0 kb and 1.0 kb from the transcription start site (TSS; Figure 5B). Then, we examined the relationship between the degree of HBO1-BRD1 binding and transcription status by using published data on expression profiles of K562 cells examined with microarrays.[21] The HBO1- or BRD1-occupied genes tended to be expressed in K562 cells (Figure 5C), indicating that the HBO1-BRD1 complex generally activates transcription of their target genes. The functional annotation of the set of genes bound by both BRD1 and HBO1 was performed on the basis of gene ontology and showed significant enrichment for genes that fell into the categories "transcriptional coactivator activity" ($P < .015$), "transcriptional factor activity" ($P < .018$), and "structural constituent of the ribosome" ($P < .042$).

Of note, targets included erythroid master regulator genes, *GATA1*, *TAL1/SCL*, and *LMO2*, and other regulator genes such as *CBFA2T3/ETO2*, *STAT5A*, and *STAT5B* (supplemental Table 1). The binding of HBO1 and BRD1 was detected throughout the coding regions of genes with peaks around TSS (Figure 5D-E).

Acetylation of H3K14 is specifically reduced in *Brd1*$^{-/-}$ mice

To test for a function of Brd1 as a histone modifier, we compared histone acetylation in CD71$^+$Ter119$^-$ and CD71$^+$Ter119$^+$ erythroblasts between *Brd1*$^{-/-}$ and *Moz*$^{-/-}$ fetal livers. Of note, the level of global acetylation of H3K14 was profoundly decreased in *Brd1*$^{-/-}$ erythroblasts by 70%-80% and that of H3K9 was also moderately decreased, whereas those of H4K5, K8, and K12 were not significantly changed (Figure 6A and supplemental Figure 6A). In contrast, the levels of global acetylation of H3K9 and H3K14 did not change in *Moz*$^{-/-}$ erythroblasts (Figure 6A). Similar results were obtained with *Brd1*$^{-/-}$ and *Moz*$^{-/-}$ mouse embryonic fibroblasts (MEFs) and *Brd1*$^{-/-}$ brain (supplemental Figure 6B-C). In contrast, the levels of representative repressive histone modifications, H3K9me3 and H3K27me3, were not largely changed in erythroblasts and MEFs (supplemental Figure 6D-E). ChIP assays confirmed global reductions in levels of H3K14 acetylation in the promoter regions of both erythroid (*Gata1*, *Stat5a*, and *Tal1*) and nonerythroid (Albumin; Alb) genes (Figure 6B). Furthermore, the ChIP-on-chip analysis in K562 revealed that H3K14 were highly acetylated at the TSS/promoter region of 46.9% of the genes bound by both BRD1 and HBO1, including *GATA1*, *TAL1/SCL*, *CBFA2T3/ETO2*, and *STAT5A* (supplemental Figure 7). These findings support our biochemical findings that BRD1 forms a HAT complex with HBO1 but not MOZ and imply that this complex is responsible for the bulk of H3K14 acetylation.

We then tested whether the depletion of HBO1 in erythroblasts recapitulates the defective erythropoiesis of *Brd1*$^{-/-}$ fetal livers. We purified c-Kit$^+$ CD71$^-$ hematopoietic progenitors from 12.5 dpc fetal livers. The cells were transduced with *Hbo1* knockdown lentiviruses and then cultured for 3 days in the presence of EPO to induce erythroid differentiation (Figure 6C). Of note, the frequency of CD71$^+$Ter119$^+$ erythroblasts in the green fluorescent protein positive (GFP$^+$) knockdown cells was significantly reduced with sh-*Hbo1*#2 and #3 (Figure 6C). Quantitative RT-PCR analysis of the erythroblasts revealed that sh-*Hbo1*#3 knocked down *Hbo1* more efficiently than #2 (#2, 44.7%, and #3, 19.1% of the control). Correspondingly, the block in erythroid differentiation was more pronounced by knockdown with #3. These results indicate that *Hbo1* knockdown perturbs differentiation of fetal liver erythroid progenitors in a fashion similar to the absence of *Brd1*. Importantly, levels of H3K14 acetylation were severely reduced in *Hbo1*-knockdown erythroblasts and H3K9 acetylation was also significantly reduced (Figure 6D). In addition, levels of H4K5 and K8 acetylation were moderately reduced in *Hbo1*-knockdown erythroblasts (Figure 6D).

We then compared the expression levels of erythroid transcription factors in wild-type and *Brd1*$^{-/-}$ erythroblasts by quantitative RT-PCR. As expected, mRNA expression of *Gata1*, *Scl/Tal1*, and *Lmo2*,[22-26] erythroid master regulator genes that appeared to be the direct targets of the HBO1-BRD1 complex in K562 cells, was mildly decreased in *Brd1*$^{-/-}$ erythroblasts (Figure 7A). Furthermore, expression of *Gata2*, the gene negatively regulated by Gata1,[27,28] was up-regulated in *Brd1*$^{-/-}$ CD71$^+$Ter119$^+$ erythroblasts. These expression patterns implied that the impaired functions of erythroid transcription factors, particularly Gata1, is responsible for the defective erythropoiesis in *Brd1*$^{-/-}$ fetal livers. To test this hypothesis, we transduced c-Kit$^+$CD71$^-$ hematopoietic progenitors from 12.5 dpc fetal livers with *Gata1* and cultured them for 3 days in the presence of EPO to induce erythroid differentiation (Figure 7B). Notably, forced expression of *Gata1* efficiently restored the proliferative capacity and survival of *Brd1*$^{-/-}$ erythroblasts (Figure 7B). Of note, however, it only partially canceled the differentiation block at the CD71$^+$Ter119$^-$ to CD71$^+$Ter119$^+$ transition (Figure 7B). Furthermore, the morphologic analyses of the purified CD71$^+$Ter119$^+$ erythroblasts revealed no obvious defects in morphologic maturation of *Brd1*$^{-/-}$ CD71$^+$Ter119$^+$ erythroblasts even in the absence of exogenous *Gata1* (supplemental Figure 8). These results suggest that dysregulated expression of *Gata1* mainly accounts for impaired proliferation and survival of *Brd1*$^{-/-}$ erythroblasts.

Discussion

In this study, we identified a novel HAT complex consisting of HBO1, BRD1, and ING4. BRD1 was believed to be involved in the MOZ HAT complex on the basis of analogy to BRPF1[3,4] but appeared to prefer to form a complex with HBO1. The finding that HBO1 stabilized the BRD1 protein further supported the physiologic significance of this complex. The levels of H3K14 acetylation were profoundly reduced in all cells and organs examined in *Brd1*$^{-/-}$ mice and *Hbo1*-knockdown erythroblasts. Thus, this

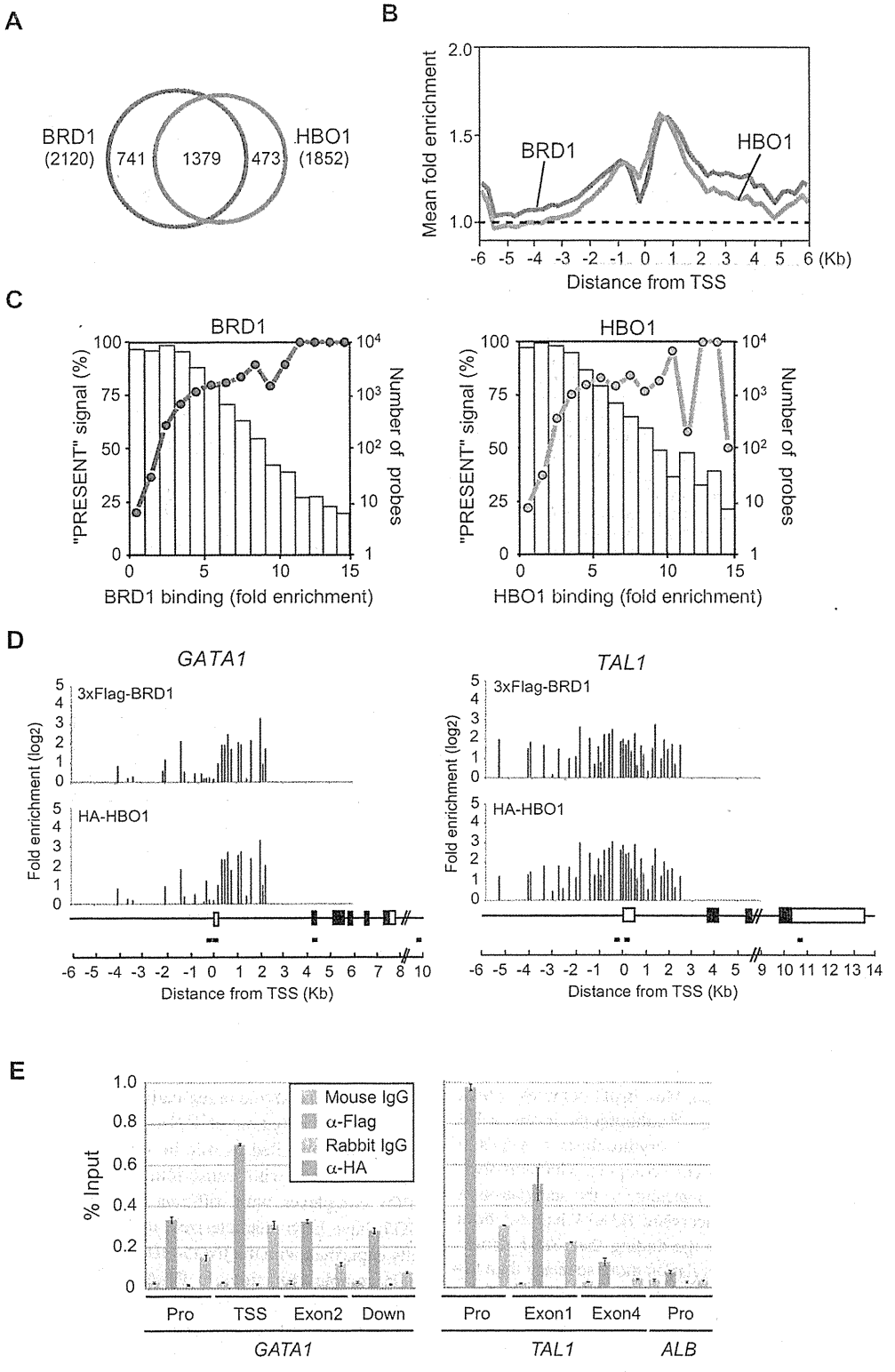

Figure 5. BRD1 and HBO1 coregulate erythroid genes. (A) ChIP-chip analysis of BRD1 and HBO1 binding in K562 cells. A ChIP-chip analysis was performed in K562 cells coexpressing 3xFlag-BRD1 and HA-HBO1 by use of anti-Flag and HA antibodies. Fold enrichment > 4 was judged as positive. The number of genes in each category of the Venn diagram is indicated. (B) Average BRD1 and HBO1 binding was depicted in the promoter regions (from −6 kb to +6 kb relative to the transcription start site) of all genes in the ChIP-on-chip analysis. The dotted line represents the normalized average signal over the entire chip. (C) Graph of the correlation of expressed genes in K562 cells in terms of the degree of BRD1 or HBO1 binding. Gene expression profiles of K562 cells examined with microarrays were used to judge the transcriptional status of the BRD1- or HBO1-occupied genes identified in the ChIP-chip analysis. The percentage of probes that produced "PRESENT" signals in the microarray analysis was plotted against the BRD1 or HBO1 binding detected in the ChIP-on-chip analysis. (D) ChIP-on-chip signals in the GATA1 and TAL1 promoter regions. Blue columns indicate the probes with no signals. The GATA1 and TAL1 gene structures and the location of the primer sets are depicted. (E) ChIP analyses at the GATA1 and TAL1 loci. The binding of BRD1 and HBO1 to the indicated regions of the GATA1 and TAL1 genes was determined by ChIP and site-specific real-time PCR. The relative amount of immunoprecipitated DNA is depicted as a percentage of input DNA. The data are shown as the mean ± SE for triplicate PCRs. The ALB promoter served as a negative control. Pro indicates promoter; and Down, 3 kb downstream from the polyadenylation site.

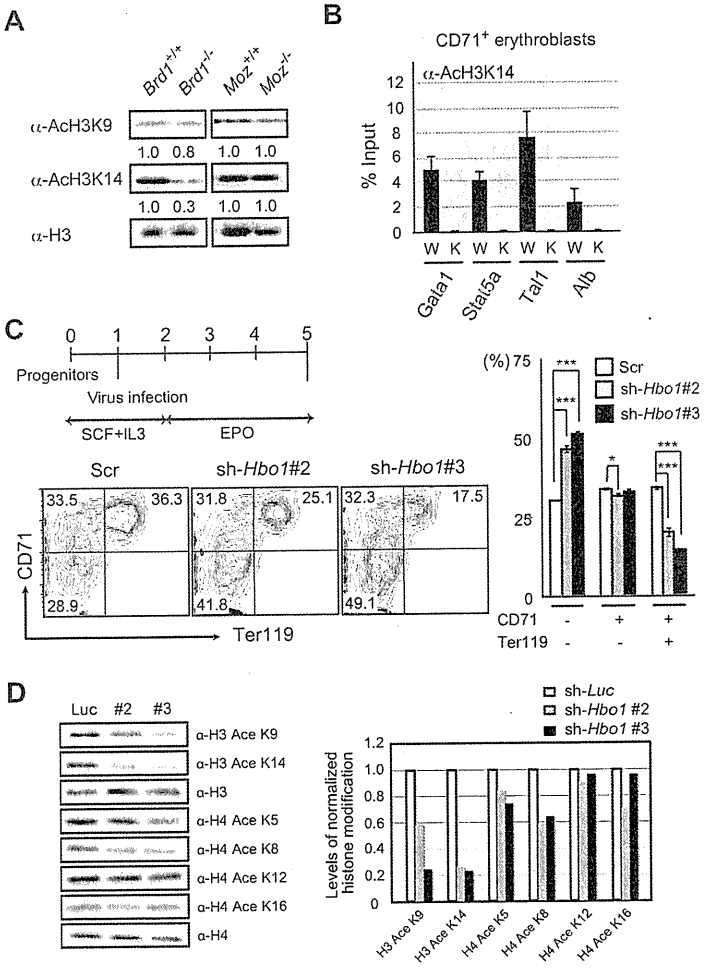

Figure 6. The Hbo1-Brd1 complex is responsible for the bulk of H3K14 acetylation. (A) Levels of acetylation at histone H3 in wild-type, *Brd1*$^{-/-}$, and *Moz*$^{-/-}$ CD71^{+}Ter119^{-} erythroblasts. Histones purified from purified CD71^{+}Ter119^{-} erythroblasts were analyzed by Western blotting by use of the indicated antibodies. Levels of acetylated H3K9 and H3K14 were normalized to the amount of H3 and are indicated relative to wild-type control values. (B) Levels of H3K14 acetylation at the promoters of erythroid regulator genes. A ChIP analysis was performed with CD71^{+} erythroblasts from wild-type (W) and *Brd1*$^{-/-}$ (K) 12.5 dpc fetal livers with an anti-acetylated H3K14 antibody. The relative amount of immunoprecipitated DNA is depicted as a percentage of input DNA. The data are shown as the mean ± SE for triplicate PCRs. The *Alb* promoter served as a negative control. (C) *Hbo1* knockdown in fetal liver progenitor cells. c-Kit^{+} CD71^{-} cells were sorted from fetal livers at 12.5 dpc and cultured in the presence of SCF and IL3. Twenty-four hours later, cells were infected with lentiviruses against *Hbo1* (#2 and #3) and the culture medium was changed to that containing EPO to induce erythroid differentiation (top left). After a 3-day induction, cells were stained with the indicated antibodies and analyzed by flow cytometry. The knockdown cells were monitored for expression of GFP, a marker antigen for infection. The flow cytometric profiles of GFP^{+} cells are indicated (bottom left) and their differentiation defined by the expression of CD71 and Ter119 is shown as the mean ± SE for triplicate cultures (right). * $P < .05$, *** $P < .0005$. (D) Levels of acetylation of histones H3 and H4 in *Hbo1*-knockdown erythroblasts. Histones were prepared from CD71^{+} erythroblasts purified from the *Hbo1*-knockdown culture in (C) and analyzed by Western blotting by the use of the indicated antibodies (left). Levels of acetylation of H3 and H4 at each residue were normalized to the amount of H3 and H4, respectively. The acetylation levels relative to the sh-*Luc* controls are indicated (right).

complex is responsible for the bulk of H3K14 acetylation in general. Very recently, loss of Hbo1 in mice was reported to lead to a significant reduction of H3K14 acetylation, but not to affect acetylation at other histone residues.[29] These observations correspond well to ours and support our notion that BRD1 functions in the HBO1 HAT complex. However, residual H3K14 acetylation was evident in *Brd1*$^{-/-}$ cells, suggesting the existence of other H3K14 HATs. These might include the Moz-Brpf1 complex, which reportedly acetylates H3K9 and K14,[7,30] although the levels of H3 acetylation were not affected in *Moz*$^{-/-}$ erythroblasts or MEFs in this study. In addition, another Hbo1 HAT complex, which involves Jade family proteins,[3,20] might also contribute to the acetylation of H3K14, although its capacity to acetylate H3K14 has not been tested. This notion is supported by the finding that *Hbo1* knockdown affected levels of H3K14 acetylation more severely than the depletion of Brd1 in erythroblasts.

HBO1 and MOZ/MORF MYST HAT complexes target chromatin via multiple PHD finger-based interactions with histone H3 tails.[5] The PHD finger of ING4 recognizes and binds to H3K4me3.[5-7] JADE and BRPF family proteins share 2 highly conserved PHD fingers that function in chromatin binding. Given their similar composition, the HBO1 and MOZ/MORF HAT complexes likely regulate acetylation of H3K14. Nonetheless, the absence of Brd1 had little or no impact on the acetylation of H3K9 and H4 (K5, K8, and K12) whereas *Hbo1* knockdown considerably affected the acetylation of H3K9 and H3K14 and marginally reduced levels of acetylated H4K5 and K8. *Jade1L* knockdown reportedly decreased bulk histone H4 acetylation in 293T cells.[20] These findings highlight differences in specificity among these HAT complexes.

HBO1 was originally cloned as a binding partner of origin recognition complex 1, a subunit of the DNA replication initiation complex, and interacts with MCM2, a component of the MCM helicase complex.[31,32] According to accumulating evidence,[3,33,34] HBO1 has a crucial role in regulation of the prereplicative complex assembly and initiation of DNA replication. In contrast, recent findings also unveiled its role in transcriptional regulation, sometimes in concert with transcription factors. Two closely related HBO1 complexes with different ING proteins (either ING4 or ING5) have been characterized and MCM proteins were specifically copurified with the ING5-HBO1 complex, suggesting that the ING5 complex functions in DNA replication whereas the ING4 complex is involved in transcriptional regulation. Actually, *ING5* knockdown in 293T cells completely blocks cell-cycle progression through the S phase.[3] Thus, composition, ie, the recruitment of either ING4 or ING5, may hold the key to context-dependent function of HBO1. BRD1 forms a complex with HBO1 and ING4 and loss of Brd1 impaired the maturation and/or survival of erythroblasts, but not their proliferation, indicating that the transcription-related function of Hbo1 is mainly affected in *Brd1*-deficient erythroid cells. However, Kueh et al[29] observed no defects in DNA replication or cell proliferation in *Hbo1* mutant embryos, MEFs, or

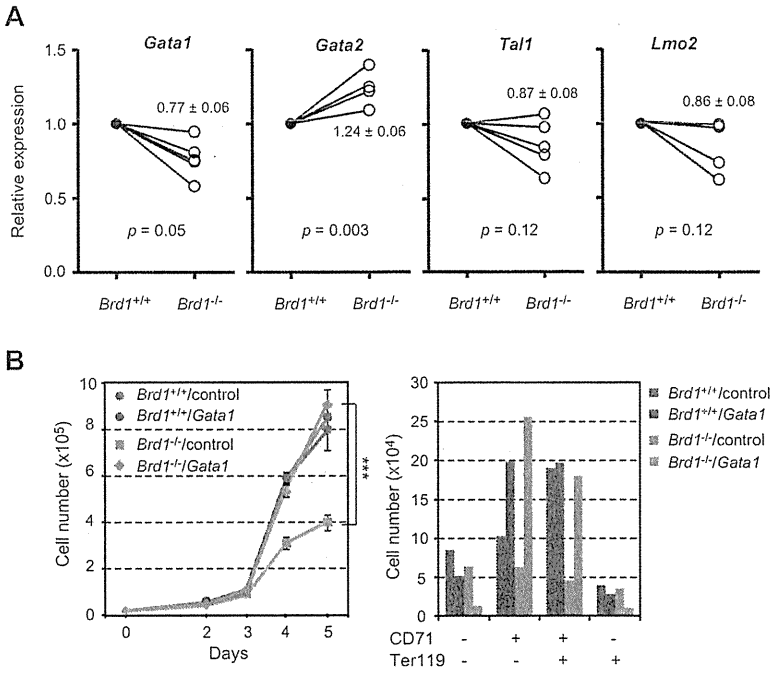

Figure 7. Insufficient transcription of erythroid regulator genes causes impaired erythropoiesis in *Brd1*$^{-/-}$ fetal livers. (A) Quantitative RT-PCR analysis of expression of erythroid transcription factor genes in erythroblasts purified from wild-type and *Brd1* $^{/}$ 12.5 dpc fetal livers. mRNA levels were normalized to *Hprt1* expression. Expression levels relative to those in the wild-type erythroblasts are shown as the mean ± SE (n = 4~5). (B) Rescue of defective proliferation of *Brd1*$^{-/-}$ erythroblasts by exogenous *Gata1*. c-Kit^{+} CD71^{-} cells were sorted from wild-type (*Brd1*$^{+/+}$) and *Brd1* $^{/}$ fetal livers at 12.5 dpc and cultured in the presence of SCF and IL-3. Twenty-four hours later, cells were infected with either *GFP* control or *Gata1* retroviruses and the culture medium was changed to that containing EPO to induce erythroid differentiation. After a 3-day induction, cells were stained with the indicated antibodies and analyzed by flow cytometry. Cell growth during culture (left) and the final numbers of erythroid cells at different stages of differentiation (CD71^{-}Ter119^{-} to CD71^{-}Te119^{+}; right) are shown as mean ± SE for triplicate cultures. ***$P < .0005$.

immortalized fibroblasts. Role of Hbo1 in DNA replication might require careful reevaluation using *Hbo1*-deficient cells.

It is widely recognized that the N-terminal tail of histone proteins is acetylated in the promoter region of actively transcribed genes and acetyl-lysine residues are recognized by bromodomain-containing factors in general. Although the role of acetylation at H3K9 and K14 is not well understood compared with that of histone methylation, H4K8 and K12 acetylation is reportedly followed by H3K9 and K14 acetylation at the IFNβ promoter after a viral infection.[35] In this cascade, H4K8 acetylation mediates recruitment of the SWI/SNF complex via the bromodomain-containing BRG1 subunit, whereas the acetylation of H3K9 and K14 is critical to the recruitment of TFIID via a tandem bromodomain factor, TAFII250. This coordinated recruitment of transcriptional complexes participates in the transcriptional induction of the *IFN-β* gene. However, the BAF complex is reported to be anchored to promoters by acetylated H3K14 though the BAF57 subunit, which contains a bromodomain.[36] Therefore, the BRD1-HBO1 complex might be involved in the recruitment of transcriptional complexes to promoters via H3K14 acetylation and exert activity in transcriptional initiation. However, the binding of BRD1 and HBO1 was detected throughout the coding regions of genes, although the peaks were detected around TSS. Therefore, we cannot eliminate a role for the HBO1 HAT complex in transcriptional elongation as proposed by Saksouk et al.[6] The recognition of H3K36me3, an epigenetic mark for transcriptional elongation, by the PWWP domain of Brpf1 supports this notion.[37]

Among the study of various developmental defects observed in *Brd1*$^{-/-}$ embryos, detailed analyses of erythropoiesis highlighted a crucial role for the HBO1-BRD1 complex in transcriptional activation of developmental regulator genes. The process of erythropoiesis is well orchestrated at the molecular level by a complex network of transcription factors, including *Gata1*, *Gata2*, and *Scl/Tal1*.[24,26] A genome-wide ChIP-chip analysis clearly demonstrated that the HBO1-BRD1 complex targets genes involved in "transcriptional regulation," including these key erythroid regulator genes. Among them, the transcription factor gene *Gata1* is required for terminal erythroid maturation and functions as an activator or repressor depending on context. *Gata1*-deficient embryos are severely anemic and their fetal liver erythroblasts have a differentiation block at the CD71^{+}Ter119^{-} stage and undergo massive apoptosis.[22-24,26] Although the reduction in *Gata1* expression was mild in *Brd1*$^{-/-}$ erythroblasts, the expression of *Gata2*, an erythroid regulator gene negatively regulated by Gata1, was mildly but significantly derepressed, and impaired *Brd1*$^{-/-}$ erythropoiesis was partially restored by the expression of *Gata1*. Given that the Hbo1-Brd1 complex regulates global H3K14 acetylation in erythroblasts, the defective erythropoiesis could not be attributed solely to *Gata1*. The failure of exogenous *Gata1* to release differentiation block of *Brd1*$^{-/-}$ erythroblasts supports this notion. Nevertheless, all these findings provide the first evidence of a crucial role for the HBO1-BRD1-ING4 complex and H3K14 acetylation in the transcriptional activation of key developmental regulator genes required for development and differentiation.

The MYST family HATs are involved in various aspects of tumorigenesis as transcriptional regulators.[1] Overexpression of HBO1 has also been reported in various human cancers.[38] Intriguingly, BRD1 fused to PAX5 (PAX5-BRD1) has recently been implicated in acute lymphoblastic leukemia.[39] This fusion protein is thought to ectopically activate transcription of PAX5 target genes by recruiting HBO1. Thus, our findings also provide a molecular basis to understanding the complex functions of HBO1 in cancer.

Acknowledgments

The authors are indebted to Drs Masayoshi Iizuka and Matthias Hammerschmidt for providing the pFLAG-HBO1 and pcDNA3-Flag-Brpf1 vectors, respectively; Makiko Yui for her technical assistance; and Drs Kiyotaka Toshimori and Tohru Mutoh for technical advice on the histochemical analyses.

This work was supported in part by MEXT KAKENHI (22118004, 20052009, 21790906, and 22118004) and for the Global COE Program (Global Center for Education and Research

in Immune System Regulation and Treatment), MEXT, Japan, a Grant-in-Aid for the Core Research for Evolutional Science and Technology (CREST) from the Japan Science and Technology Corporation (JST), and a grant from the Takeda Science Foundation.

Authorship

Contribution: Y.M., S.M., and A.S. performed the experiments, analyzed results, made the figures, and wrote the manuscript; M.N. cloned Brd1 cDNA; M.E., T.A.E., and T.T. performed the ChIP-chip assay; J.S. and H.K. generated *Brd1*-deficient mice; T.K. and I.K. provided *Moz*-deficient mice and prepared *Moz*-deficient MEFs; T.C. performed phenotypic analysis of *Brd1*-deficient mice; N.Y. gave a critical suggestion to the project; and A.I. conceived of and directed the project, secured funding, and wrote the manuscript.

Conflict-of-interest disclosure: The authors declare no competing financial interests.

Correspondence: Atsushi Iwama, MD, PhD, 1-8-1 Inohana, Chuo-ku, Chiba, 260-8670 Japan; e-mail: aiwama@faculty.chiba-u.jp.

References

1. Avvakumov N, Côté J. The MYST family of histone acetyltransferases and their intimate links to cancer. *Oncogene.* 2007;26(37):5395-5407.
2. Lee KK, Workman IL. Histone acetyltransferase complexes: one size doesn't fit all. *Nat Rev Mol Cell Biol.* 2007;8(4):284-295.
3. Doyon YC, Cayrou M, Ullah AJ, et al. ING tumor suppressor proteins are critical regulators of chromatin acetylation required for genome expression and perpetuation. *Mol Cell.* 2006;21(1):51-64.
4. Ullah M, Pelletier N, Xiao L, et al. Molecular architecture of quartet MOZ/MORF histone acetyltransferase complexes. *Mol Cell Biol.* 2008; 28(22):6828-6843.
5. Hung T, Binda O, Champagne KS, et al. ING4 mediates crosstalk between histone H3 K4 trimethylation and H3 acetylation to attenuate cellular transformation. *Mol Cell.* 2009;33(2):248-256.
6. Saksouk N, Avvakumov N, Champagne KS, et al. HBO1 HAT complexes target chromatin throughout gene coding regions via multiple PHD finger interactions with histone H3 tail. *Mol Cell.* 2009; 33(2):257-265.
7. Taverna SD, Ilin S, Rogers RS, et al. Yng1 PHD finger binding to H3 trimethylated at K4 promotes NuA3 HAT activity at K14 of H3 and transcription at a subset of targeted ORFs. *Mol Cell.* 2006; 24(5):785-796.
8. Katsumoto T, Aikawa Y, Iwama A, et al. MOZ is essential for maintenance of hematopoietic stem cells. *Genes Dev.* 2006;20(10):1321-1330.
9. Thomas T, Corcoran LM, Gugasyan R, et al. Monocytic leukemia zinc finger protein is essential for the development of long-term reconstituting hematopoietic stem cells. *Genes Dev.* 2006; 20(9):1175-1186.
10. Crump JG, Swartz ME, Eberhart JK, Kimmel CB. Moz-dependent Hox expression controls segment-specific fate maps of skeletal precursors in the face. *Development.* 2006;133(14):2661-2669.
11. Laue K, Daujat S, Crump JG, et al. The multidomain protein Brpf1 binds histones and is required for Hox gene expression and segmental identity. *Development.* 2008;135(11):1935-1946.
12. Hibiya K, Katsumoto T, Kondo T, Kitabayashi I, Kudo A. Brpf1, a subunit of the MOZ histone acetyl transferase complex, maintains expression of anterior and posterior Hox genes for proper patterning of craniofacial and caudal skeletons. *Dev Biol.* 2009;329(2):176-190.
13. McCullagh P, Chaplin T, Meerabux J, et al. The cloning, mapping and expression of a novel gene, BRL, related to the AF10 leukaemia gene. *Oncogene.* 1999;18(52):7442-7452.
14. Kitamura T, Koshino Y, Shibata F, et al. Retrovirus-mediated gene transfer and expression cloning: powerful tools in functional genomics. *Exp Hematol.* 2003;31(11):1007-1014.
15. Iwama A, Oguro H, Negishi M, et al. Enhanced self-renewal of hematopoietic stem cells mediated by the polycomb gene product, Bmi-1. *Immunity.* 2004;21(6):843-851.
16. Katayama K, Wada K, Miyoshi H, et al. RNA interfering approach for clarifying the PPARgamma pathway using lentiviral vector expressing short hairpin RNA. *FEBS Lett.* 2004;560(1-3):178-182.
17. Kitabayashi I, Aikawa Y, Nguyen LA, Ohki M. Activation of AML1-mediated transcription by MOZ and inhibition by the MOZ-CBP fusion protein. *EMBO J.* 2001;20(24):7184-7196.
18. Kimura H, Hayashi-Takanaka Y, Goto Y, Takizawa N, Nozaki N. The organization of histone H3 modifications as revealed by a panel of specific monoclonal antibodies. *Cell Struct Funct.* 2008;33(1):61-73.
19. Endoh M, Endo TA, Endoh T, et al. Polycomb group proteins Ring1A/B are functionally linked to the core transcriptional regulatory circuitry to maintain ES cell identity. *Development.* 2008; 135(8):1513-1524.
20. Foy RL, Song IY, Chitalia VC, et al. Role of Jade-1 in histone acetyltransferase (HAT) HBO1 complex. *J Biol Chem.* 2008;283(43):28817-28826.
21. Addya S, Keller MA, Delgrosso K, et al. Erythroid-induced commitment of K562 cells results in clusters of differentially expressed genes enriched for specific transcription regulatory elements. *Physiol Genomics.* 2004;19(1):117-130.
22. Pevny L, Simon MC, Robertson E, et al. Erythroid differentiation in chimaeric mice blocked by a targeted mutation in the gene for transcription factor GATA-1. *Nature.* 1991;349(6306):257-260.
23. Weiss MJ, Orkin SH. Transcription factor GATA-1 permits survival and maturation of erythroid precursors by preventing apoptosis. *Proc Natl Acad Sci U S A.* 1995;92(21):9623-9627.
24. Cantor AB, Orkin SH. Transcriptional regulation of erythropoiesis: an affair involving multiple partners. *Oncogene.* 2002;21(21):3368-3376.
25. Mikkola HK, Klintman J, Yang H, et al. Haematopoietic stem cells retain long-term repopulating activity and multipotency in the absence of stem-cell leukaemia SCL/tal-1 gene. *Nature.* 2003; 421(6922):547-551.
26. Kaneko H, Shimizu R, Yamamoto M. GATA factor switching during erythroid differentiation. *Curr Opin Hematol.* 2010;17(3):163-168.
27. Grass JA, Boyer ME, Pal S, Wu J, Weiss MJ, Bresnick EH. GATA-1-dependent transcriptional repression of GATA-2 via disruption of positive autoregulation and domain-wide chromatin remodeling. *Proc Natl Acad Sci U S A.* 2003; 100(15):8811-8816.
28. Fujiwara T, O'Geen H, Keles S, et al. Discovering hematopoietic mechanisms through genome-wide analysis of GATA factor chromatin occupancy. *Mol Cell.* 2009;36(4):667-681.
29. Kueh AJ, Dixon AP, Voss AK, Thomas T. HBO1 is required for H3K14 acetylation and normal transcriptional activity during embryonic development. *Mol Cell Biol.* 2011;31(4):845-860.
30. Voss AK, Collin C, Dixon MP, Thomas T. Moz and retinoic acid coordinately regulate H3K9 acetylation, Hox gene expression, and segment identity. *Dev Cell.* 2009;17(5):674-686.
31. Iizuka M, Stillman B. Histone acetyltransferase HBO1 interacts with the ORC1 subunit of the human initiator protein. *J Biol Chem.* 1999;274(33): 23027-23034.
32. Burke TW, Cook JG, Asano M, Nevins JR. Replication factors MCM2 and ORC1 interact with the histone acetyltransferase HBO1. *J Biol Chem.* 2001;276(18):15397-15408.
33. Iizuka M, Matsui T, Takisawa H, Smith MM. Regulation of replication licensing by acetyltransferase Hbo1. *Mol Cell Biol.* 2006;26(3):1098-1108.
34. Miotto B, Struhl K. HBO1 histone acetylation is a coactivator of the replication licensing factor Cdt1. *Genes Dev.* 2008;22(19):2633-2638.
35. Agalioti T, Chen G, Thanos D. Deciphering the transcriptional histone acetylation code for a human gene. *Cell.* 2002;111(3):381-392.
36. Vicent GP, Zaurin R, Nacht AS, et al. Two chromatin remodeling activities cooperate during activation of hormone responsive promoters. *PLoS Genet.* 2009;5(7):e1000567.
37. Vezzoli A, Bonadies N, Allen MD, et al. Molecular basis of histone H3K36me3 recognition by the PWWP domain of Brpf1. *Nat Struct Mol Biol.* 2010;17(5):617-619.
38. Iizuka M, Takahashi Y, Mizzen CA, et al. Histone acetyltransferase Hbo1: catalytic activity, cellular abundance, and links to primary cancers. *Gene.* 2009;436(1-2):108-114.
39. Nebral K, Denk D, Attarbaschi A, et al. Incidence and diversity of PAX5 fusion genes in childhood acute lymphoblastic leukemia. *Leukemia.* 2009; 23(1):134-143.

THE JOURNAL OF BIOLOGICAL CHEMISTRY VOL. 286, NO. 20, pp. 18251–18260, May 20, 2011

Cancer Susceptibility Polymorphism of p53 at Codon 72 Affects Phosphorylation and Degradation of p53 Protein*[S]

Received for publication, December 14, 2010, and in revised form, March 18, 2011 Published, JBC Papers in Press, March 28, 2011, DOI 10.1074/jbc.M110.208587

Chikako Ozeki,[a,b,c] Yuichiro Sawai,[d,e] Tatsuhiro Shibata,[f] Takashi Kohno,[g] Koji Okamoto,[a,h] Jun Yokota,[g] Fumio Tashiro,[e] Sei-ichi Tanuma,[c] Ryuichi Sakai,[i] Tatsuya Kawase,[a,e] Issay Kitabayashi,[b] Yoichi Taya,[a,j1] and Rieko Ohki[a,d,j2]

From the [a]Radiobiology Division, [b]Molecular Oncology Division, [f]Division of Cancer Genomics, [g]Biology Division, [h]Early Oncogenesis Research Project, [i]Growth Factor Division, [d]Division of Cancer Biology, National Cancer Center Research Institute, Tsukiji 5-1-1, Chuo-ku, Tokyo 104-0045, Japan, the [e]Department of Biological Science and Technology, Faculty of Industrial Science and Technology, [c]Department of Biochemistry, Faculty of Pharmaceutical Sciences, Tokyo University of Science, Yamazaki 2641, Noda-shi, Chiba 270-8510, Japan, and the [j]Cancer Science Institute of Singapore and Department of Biochemistry, National University of Singapore, Center for Life Sciences 02-07, Medical Drive, 117456, Singapore

The common polymorphism of p53 at codon 72, either encoding proline or arginine, has drawn attention as a genetic factor associated with clinical outcome or cancer risk for the last 2 decades. We now show that these two polymorphic variants differ in protein structure, especially within the N-terminal region and, as a consequence, differ in post-translational modification at the N terminus. The arginine form (p53-72R) shows significantly enhanced phosphorylation at Ser-6 and Ser-20 compared with the proline form (p53-72P). We also show diminished Mdm2-mediated degradation of p53-72R compared with p53-72P, which is at least partly brought about by higher levels of phosphorylation at Ser-20 in p53-72R. Furthermore, enhanced p21 expression in p53-72R-expressing cells, which is dependent on phosphorylation at Ser-6, was demonstrated. Differential p21 expression between the variants was also observed upon activation of TGF-β signaling. Collectively, we demonstrate a novel molecular difference and simultaneously suggest a difference in the tumor-suppressing function of the variants.

The *p53* gene is a tumor suppressor gene, and loss of functional p53 is the most common anomaly found in human cancers (1). Signals activated upon various cellular stresses stabilize and activate p53, which exerts its tumor-suppressive function mainly by acting as a transcriptional activator. Target genes of p53 regulate a variety of processes, such as the induction of cell cycle arrest, cell death, DNA repair and senescence, and function downstream of p53 to prevent tumorigenesis (2). Depending on the stress signal, p53 selectively activates its target genes to implement various p53-mediated responses. Post-translational modification of p53 is a candidate mechanism that causes p53 to respond to different stress signals, and phosphorylation of p53 is the most major post-translational modification of p53 (3, 4). Kinases activated upon cellular stress, such as ataxia telangiectasia-mutated (ATM), ataxia telangiectasia and Rad3-related (ATR), and p38, phosphorylate serine and threonine residues, and phosphorylation results in the activation of p53 protein (5).

The structure of p53 protein is commonly divided into three functional domains as follows: the N-terminal domain, central core DNA-binding domain, and C-terminal domain. The N-terminal domain is required for the transcriptional activity of p53 protein and consists of two transactivation domains and a proline-rich domain. The transactivation domains are extensively phosphorylated upon p53 activation. Seven serines, Ser-6, -9, -15, -20, -33, -37, and -46, within the transactivation domain undergo phosphorylation (6). Phosphorylation of each residue has been reported to have specific physiological significance; for example, phosphorylation of Ser-15 or -46 modifies the transactivation ability of p53 (7–9), whereas Ser-20 is required for p53 protein stability (10). When not phosphorylated, p53 is actively degraded by the 26 S proteasome pathway by interacting with a ring finger ubiquitin E3 ligase, Mdm2. Upon activation, p53 is phosphorylated at Thr-18 and Ser-20, both of which reside within the Mdm2 binding domain, leading to reduced affinity with Mdm2 and escape from ubiquitination and subsequent degradation (11).

The proline-rich domain functions as a protein-protein interaction domain, and several proteins that bind to this region have been reported (12, 13). In particular, five P*XXP* motifs appearing in this domain are known to be critical for the interaction with Src homology 3 domain-containing proteins. In addition, within the proline-rich domain, a common polymorphism of p53 at codon 72, encoding either proline or arginine (p53-72P or p53-72R), has been reported (14–16). Notably, the proline at residue 72 of p53 is part of a P*XXP* motif, and

* This work was supported by grants-in-aid for scientific research from the Ministry of Education, Culture, Sports, Science, and Technology of Japan (to R. O., T. K., and Y. T.), grants-in-aid for the Third Term Comprehensive Ten-year Strategy for Cancer Control from the Ministry of Health, Labor, and Welfare Japan (to T. S., J. Y., and Y. T.), Program for Promotion of Fundamental Studies in Health Sciences of the National Institute of Biomedical Innovation (to T. S., T. K., and J. Y.), New Energy and Industrial Technology Development Organization (to R. O.), research grants from Hayashi Memorial Foundation for Female Natural Scientists (to R. O.), the Sagawa Foundation for Promoting Cancer Research (to R. O.), Takeda Science Foundation (to R. O.), Kobayashi Foundation for Cancer Research (to R. O.), and the Mochida Memorial Foundation for Medical and Pharmaceutical Research (to R. O.).

[S] The on-line version of this article (available at http://www.jbc.org) contains supplemental Figs. S1–S6.

[1] To whom correspondence may be addressed. E-mail: csiyt@nus.edu.sag.
[2] To whom correspondence may be addressed. Tel.: 81-3-3542-2511 (Ext. 4304); Fax: 81-3-3542-8170; E-mail: rohki@ncc.go.jp.

therefore it can be assumed that the polymorphism will affect protein-binding partners. Extensive studies have been carried out to investigate the link between the expression of p53 polymorphic variants at codon 72 and cancer susceptibility (17). It has been reported that in a number of cancers, including lung and breast, patients with the p53-72P allele are more susceptible to cancer development and a poor clinical outcome (18–21); however, the mechanistic basis for this bias is still an open question.

To determine the functional difference of the two variant proteins p53-72R and p53-72P, we first analyzed the protease accessibility of p53-72R and p53-72P, and we found that the higher order structures are different between them. We have also found that the phosphorylation modifications of both variants are different, leading to differential protein stability and transactivation ability of the two variants.

EXPERIMENTAL PROCEDURES

Plasmids—For p53 constructs, each p53 was cloned in pcDNA3 or pMX vector as described (22). When cloned in pMX vector, each p53 is under the control of a weak retroviral LTR promoter. Constitutively active TGF-β receptor I was constructed by introducing a point mutation at codon 204 (T204D) and cloned in pcDNA3. FLAG-tagged human wild-type Mdm2 (pSG-F-Hdm2), N-terminally c-Myc tagged Mdm2 (pCMV-Myc-Mdm2), and histidine-tagged ubiquitin expression plasmids were described previously (23).

Expression and Purification of Glutathione S-Transferase (GST) Fusion Proteins—GST fusion constructs of p53-72P and -72R were prepared by PCR tagging of p53 cDNA with BamHI and XhoI sites at the 5′ and 3′ ends, respectively, and subcloned into pGEX-6P-1 vector (Amersham Biosciences). Constructs were expressed in *Escherichia coli* (BL21-Gold (DE3) Competent Cell; Stratagene, CA) and purified from cell lysates using glutathione-Sepharose 4B beads (Amersham Biosciences). Purified proteins were further digested with PreScission protease (Amersham Biosciences) to cleave p53 from GST.

Cell Culture, Transfection, and Establishment of Stable Cell Lines—Cell culture was performed as described (22). Transient transfection assays were performed using Lipofectamine Plus or Lipofectamine 2000 reagent (Invitrogen), as indicated in the figure legends. Stable HCT116 p53(−/−) cell lines expressing p53-72P or -72R were obtained by infecting cells with recombinant retroviruses. In each case, as the control cell line, cells were also infected with empty retroviruses expressing only the drug resistance gene. Infection was performed in the presence of Polybrene (at 4 μg/ml; Sigma), and subsequently, cells were selected in puromycin (at 0.5 μg/ml; Sigma). To avoid possible disadvantages from utilizing clonal cell lines, *i.e.* clonal differences, cell lines were maintained as mass cultures.

Western Blotting Analysis and Immunoprecipitation—Cells were lysed in lysis buffer containing 50 mM Tris-HCl (pH 8.0), 1% Nonidet P-40, 250 mM NaCl, 50 mM NaF, 1 mM Na_3VO_4, 1 mM protease inhibitor (PMSF, aprotinin, and leupeptin), and 1 mM DDT. Whole cell lysates were subjected to protein quantification and subjected to immunoprecipitation or analyzed by Western blotting. The antibodies used in this study were as follows: anti-p53 goat polyclonal antibody (FL393); anti-p21 rabbit polyclonal antibody (C-19); anti-PIG3 (N-20) and PIG3 (C-20) goat polyclonal antibody; anti-Bax (N-20) mouse monoclonal antibody; anti-c-Myc mouse monoclonal antibody (9E10) and anti-β-actin mouse monoclonal antibody (Santa Cruz Biotechnology, Santa Cruz, CA); penta-His antibody (Qiagen, Valencia, CA); anti-p53 mouse monoclonal antibodies PAb1801 and PAb421 and anti-Mdm2 mouse monoclonal antibody (clone IF-2) (Calbiochem); anti-p53 mouse monoclonal antibody (PAb122) (Monosan, Uden, Netherlands); anti-phospho-p53 (Ser-6, -9, -15, -20, -37, and -46) rabbit polyclonal antibodies and anti-phospho-Smad2 (138D4) Ser-465/467 antibody (Cell Signaling, Beverly, MA); anti-CRP1 antibody (BD Transduction Laboratories); and anti-FLAG mouse monoclonal antibody (M2); and anti-tubulin antibody (clone B-5-1-2) (Sigma). To detect total p53, anti-p53 goat polyclonal antibody (FL393) was used in all cases.

Northern Blotting Analysis—RNA was prepared using an RNeasy Midi kit (Qiagen). Northern blotting was performed as described (22). Probes were prepared using a BcaBEST labeling kit (TaKaRa, Kyoto, Japan) and purified by serial purification using a Probe Quant G-50 MicroColumn (Amersham Biosciences) and NICK column (Amersham Biosciences). The full open reading frame of p53 was used for probe preparation.

Detection of Ubiquitinated p53—To detect efficiently the ubiquitinated p53, Mdm2 expression vector pSG-FLAG-Mdm2 was used, in which Mdm2 was expressed from an SV40 promoter (much weaker than CMV promoter). pcDNA3-p53-72P or -72R (0.35 μg), together with His_6-tagged ubiquitin (2.2 μg) and N-terminally FLAG-tagged Mdm2 (pSG-FLAG-Mdm2, 1.42 μg) or control empty vector (1.42 μg), were introduced into H1299 cells (6×10^5 cells/10-cm dish). Cells were harvested 27 h post-transfection. Cell lysates were prepared in the presence of 1 mg/ml *N*-methylmaleimide (Sigma) to avoid degradation of ubiquitinated p53. Ubiquitinated and nonubiquitinated p53 were immunoprecipitated with anti-p53 polyclonal antibody (FL393) and analyzed by Western blotting.

^{35}S Pulse-Chase—H1299 cells (4×10^5 cells/10-cm dish) were transfected with 4 μg of plasmids with a 1:9 ratio of pcDNA-p53-72P or 72R/pCMV-Myc-Mdm2. At 19.5 h after transfection, cells were starved for 30 min in methionine- and cysteine-free DMEM with dialyzed serum and then labeled with 4.1 MBq/ml EXPRE^{35}S^{35}S ^{35}S-protein labeling mix (PerkinElmer Life Sciences) for 30 min. Cells were then cultured for 1.5 h in chase medium containing 500 μg/ml methionine and 500 μg/ml cysteine. Following incubation, cells were collected at the indicated times. Whole cell lysates were prepared from the collected cells, and immunoprecipitation was performed using anti-p53 mouse monoclonal antibodies PAb1801 and PAb421, run on SDS-PAGE, and detected by autoradiography.

Analysis of p53 Single Nucleotide Polymorphism and the Copy Number of the mdm2 Gene by Array-based Comparative Genomic Hybridization—To analyze p53 single nucleotide polymorphisms, a 10- or 20-ml whole blood sample was obtained from each individual. Genomic DNA was isolated and subjected to genotyping for p53 single nucleotide polymorphism by pyrosequencing, as described previously (19). For

array-based comparative genomic hybridization, 62 surgical specimens of lung cancer patients who had been diagnosed and had undergone surgery at the National Cancer Center Hospital were analyzed by MCG cancer array-800 comparative genomic hybridization, as described previously (24). MCG Cancer array-800 is a custom-made array consisting of ~800 BACs harboring 800 known cancer-related genes, intended for diagnosis of cancer-specific copy number aberrations. When the signal ratio (test signal/reference signal) for the copy number of the *mdm2* gene was more than 1.25, it was defined as chromosomal gain. The threshold for chromosomal gain (ratio >1.25) was determined previously by "normal *versus* normal experiments" (24).

RESULTS

N-terminal Structures of p53-72P and -72R Protein Are Different—The polymorphism of p53 at codon 72 was first reported over 2 decades ago as a non-tumor-derived amino acid change that altered the mobility of p53 on SDS-polyacrylamide gels (14–16). As shown in supplemental Fig. S1, *A* and *B*, altered mobilities of ectopically expressed, endogenously expressed, and purified p53-72P and -72R were similarly detected by Western blotting. Because purified p53 proteins prepared from *E. coli* do not undergo post-translational modifications (data not shown), the altered mobility is not due to such modifications but to the intrinsic nature of the proteins. It has been suggested that this altered mobility reflects the altered structure of the protein by amino acid change; however, because structural information about this domain is lacking, this hypothesis has not been tested. We therefore tried to test this hypothesis by partial proteolytic digestion of purified p53-72P and -72R protein. When a protein is partially digested by proteases, a difference in the protein structure is detected as sensitivity to protease digestion at each cleavage site. To observe intrinsic differences between p53-72P and -72R proteins, we used purified proteins prepared from *E. coli*. As shown in Fig. 1*A*, the products of partial proteolysis by subtilisin were analyzed by Western blotting using anti-p53 antibodies, detecting different positions within the p53 protein. We first recognized that fragments showing altered mobility between p53-72P and -72R were detected even after proteolytic digestion (Fig. 1*A*, *open circles*). Such fragments were frequently detected by the antibody detecting N-terminal p53 (Pab1801), and this demonstrates that N-terminal fragments contain a region causing electrophoretic mobility differences. However, when the antibody detecting C-terminal p53 was used (Pab122), most fragments showed the same migration, showing that the C-terminal portion of p53-72P and -72R is indistinguishable by SDS-PAGE. In addition to these fragments, the analysis revealed two bands detected only in p53-72R (Fig. 1*A*, 22- and 34-kDa bands, shown with *arrows*). As shown in Fig. 1*B*, most of the estimated digestion sites for these bands lie within the N-terminal half of p53, demonstrating that a difference in protease accessibility is frequently observed in the N-terminal p53. We also performed the same experiment using Pab240 (which detects 211–220 amino acids of p53 protein), and we found that the 22-kDa band is not detected by Pab240, suggesting the N-terminal origin of the fragment (data not shown). Unfortunately, several bands appeared around 34 kDa, and we could not verify whether a

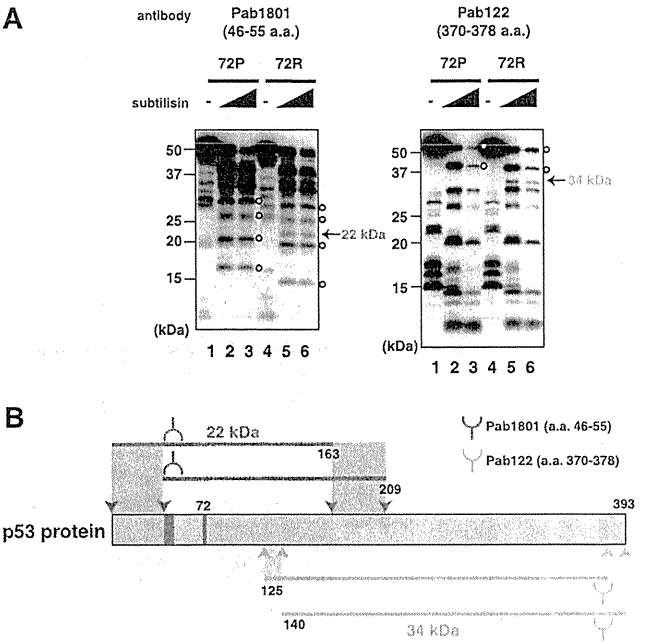

FIGURE 1. **Partial proteolytic digestion of purified p53-72P and -72R.** *A*, 35 ng of purified p53-72P or -72R were digested with subtilisin at 0.5 μg/ml (*lanes 2* and *5*) and at 1 μg/ml (*lanes 3* and *6*) for 30 min on ice. Products were resolved by 15–25% SDS-PAGE and analyzed by Western blotting using the indicated antibodies. Bands with a different proteolytic pattern (specifically observed for p53-72R) are shown by *arrows*. Note that when using antibody against N-terminal positions of p53 (Pab1801), fragments showing altered mobility on the gel between p53-72P and -72R are frequently detected (*open circles*). *B*, estimated digestion sites for p53-72R-specific bands. Schematic representation of p53 protein (*gray*) together with recognition sites for Pab1801 (*green*) and Pab122 (*yellow*) is shown. Polymorphic codon 72 is shown in *red*. The *upper two green bars* (22-kDa band in *panel Pab1801*) and *lower two yellow bars* (34-kDa band in *panel Pab122*) are the estimated alignments of p53-72R-specific fragments. The estimated amino acid numbers of the fragments were calculated according to the molecular weight of the fragments. The fragments were detected by antibodies and therefore should be derived from somewhere between the two bars. It can be assumed that p53-72R-specific digestion occurred between the *arrowheads*.

34-kDa p53-72R-specific band is detected by Pab240 (data not shown). These results collectively indicate that differences in protein structure are mainly detected in the N-terminal portion of p53.

Phosphorylation in N-terminal p53 Is Enhanced in p53-72R Compared with -72P—We next speculated that the difference in the protein structure between the variants might affect the association with the kinases that phosphorylate p53. Because the structural differences of p53-72P and -72R are mainly detected in the N-terminal region, we analyzed the phosphorylation levels of p53-72P and -72R within the N-terminal domain. We reasoned that subtle differences between the variants become evident only when they are expressed within cells having the same genetic background; therefore, we analyzed the phosphorylation levels of p53-72P and -72R by transfecting them into a cell line with no p53 (Saos2 cells). In addition, to exclude the possibility that p53 expressed in the cells is unnaturally high, each p53 was expressed from a weak retroviral LTR promoter. As shown in Fig. 2, phosphorylation levels of p53-72P and -72R were similar on Ser-9, -15, -37, and -46. However, significantly enhanced phosphorylation of 72R compared with 72P at Ser-6 and -20 was detected. Phosphorylation in the

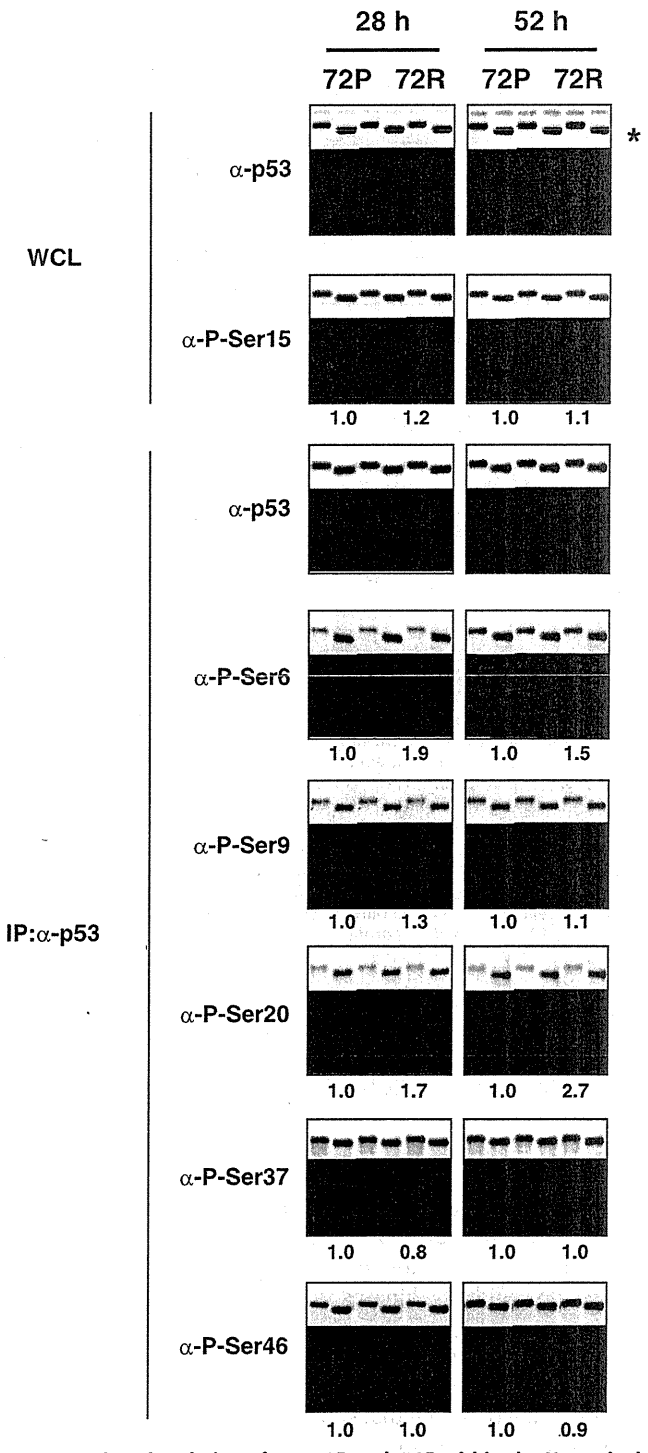

FIGURE 2. **Phosphorylation of p53-72P and -72R within the N-terminal transactivation domain.** Saos2 cells (4.4×10^6 cells/10-cm dish) were transfected with pMX-p53-72P or -72R (1.78 μg), and harvested 28 and 52 h post-transfection. To detect the phosphorylation of p53 efficiently (except Ser-15), p53 proteins were immunoprecipitated (*IP*) using anti-p53 antibodies (anti-p53 mouse monoclonal antibody pAb1801 and pAb421 were mixed). Total p53 and phosphorylated p53 were analyzed by Western blotting. The experiment was repeated three times, and representative images are shown. The phosphorylation levels of p53-72P and -72R were quantified using Image J software. Relative phosphorylation levels (normalized by total p53) are shown *below* the panels. *Asterisk* denotes a nonspecific band. *WCL*, whole cell lysate.

N-terminal region of p53 is closely related with p53 activity. We therefore analyzed whether enhanced phosphorylation at Ser-6 and -20 in p53-72R results in enhanced tumor-suppressing function of the protein, as shown below.

Stability of p53-72R Is Increased Compared with p53-72P—Phosphorylation at Ser-20 mediates the stabilization of the p53 protein by inhibiting p53-Mdm2 interaction (11). Because we detected enhanced phosphorylation at Ser-20 in p53-72R compared with p53-72P, we focused on the stability of p53 proteins expressed within the cell. We first expressed the variants at different expression levels (200–1200 ng of p53 expression vectors transfected per 10-cm dish). We speculated that if the differences in protein levels were due to differences in degradation levels by endogenous Mdm2, increased expression of p53 would override degradation by Mdm2. As shown in Fig. 3*A*, when both p53s were expressed at relatively high levels (800 or 1200 ng of p53 expression vectors transfected per 10-cm dish), no difference in total p53 levels was detected, whereas when the expression levels were decreased (200 or 400 ng transfected), p53-72R was expressed at a significantly higher level than p53-72P. The mRNA expression levels of both variants were similar even when p53-72R protein was expressed at a significantly higher level than p53-72P protein in H1299 and Saos2 cells (Fig. 3*B*); therefore, the difference in the p53 protein amount is regulated at the post-transcriptional level. We further tested whether this difference could be detected in cells lacking Mdm2. We utilized *p53* and *mdm2* double-deficient mouse embryonic fibroblasts (*p53*/*mdm2* DKO)[3] for this purpose. As shown in Fig. 3*C*, no difference in p53 protein levels was detected in *p53*/*mdm2* DKO (under the conditions utilized, expression levels of p53 variants were similar or lower than in H1299 cells, data not shown).

We next tested whether the difference in protein expression levels was affected by phosphorylation at Ser-20, which was converted to alanine in p53-72P and -72R to obtain nonphosphorylatable p53 at Ser-20 (therefore is degradable by Mdm2), and expressed in H1299 and *p53*/*mdm2* DKO. As shown in Fig. 3*D*, significant decreases in protein levels were detected for S20A mutants compared with wild-type p53s in H1299 cells. However, no such decreases were detected in *p53*/*mdm2* DKO, indicating that diminished expression levels of S20A mutants in H1299 is a result of enhanced degradation of the mutants by Mdm2. The level of S20A mutant for p53-72P was still slightly lower than p53-72R in H1299 cells, demonstrating that, in addition to phosphorylation at Ser-20, other factors may affect the difference in protein expression levels. Collectively, these results suggest that the difference in p53 protein expression levels is the result of a difference in the degradation levels of p53-72R and -72P by Mdm2, and this difference has been brought about at least partly from differences in phosphorylation levels at Ser-20.

Mdm2 Degrades p53-72P More Efficiently than p53-72R—We further tested whether there is a difference in protein degradation by Mdm2 between polymorphic variants. We first co-transfected Mdm2 with p53-72R or -72P in H1299 cells. As

[3] The abbreviations used are: DKO, double KO; ca., constitutively active.